PHILOSOPHICAL TRANSACTIONS OF THE ROYAL SOCIETY A MATHEMATICAL, PHYSICAL & ENGINEERING SCIENCES

Dynamic Features of Combustion

A. K. Oppenheim

Phil. Trans. R. Soc. Lond. A 1985 **315**, 471-508
doi: 10.1098/rsta.1985.0053

Phil. Trans. R. Soc. Lond. A **315**, 471–508 (1985) [471]
Printed in Great Britain

DYNAMIC FEATURES OF COMBUSTION

By A. K. Oppenheim
College of Engineering, Mechanical Engineering, University of California, Berkeley, California 94720, *U.S.A.*
and Lawrence Berkeley Laboratory, University of California, Berkeley, California 94720, *U.S.A.*

(*Communicated by Sir Owen Saunders, F.R.S. – Received 4 November* 1983)

[Plates 1–6]

CONTENTS

The dynamic features of combustion arise from the evolution of exothermic energy and its deposition in the essentially compressible medium in which the process takes place. These features are exposed in representative cases that cover a wide spectrum of combustion phenomena, namely ignition, flame propagation, explosion, and detonation. Ignition and explosion are treated as problems in nonlinear mechanics

dynamic properties of the system. Consideration of the turbulent flame propagation where the transformation to phase coordinates is instrumental in revealing the mechanism introduces a fascinating branch of combustion science: the aerodynamics of flames, a time-dependent treatment of the flow field where the unburnt and burnt mixtures are considered as incompressible media separated by an interface representing the flame front. The account of detonation phenomena is restricted to just the phenomenological aspects of their development and structure, illustrating vividly most of the dynamic features of combustion. Since they display the mechanism of feedback exerted by the combustion process on the flow field of the reacting medium, their study should be of particular significance to the development of controlled combustion systems: one of the most exciting prospects for energy conversion technology.

Introduction

Combustion is essentially an oxidation process that occurs predominantly in a gaseous medium. Its dynamic features are caused by the exothermicity of the oxidation reaction (a property without which combustion would have been of no practical interest). Here these features are exposed in four prominent cases, relevant to a wide spectrum of combustion phenomena, namely:

1. *ignition*: the initiation of a self-sustained exothermic process, considered in the simplest case of a closed thermodynamic system and its stochastic distribution;
2. *inflammation*: the initiation and propagation of self-sustained flames, presented in the most interesting case of turbulent flow;
3. *explosion*: the dynamic effects caused by the deposition of exothermic energy in a compressible medium, illustrated by two classical examples: self-similar blast waves with energy deposition at the front and the adiabatic non-self-similar wave;
4. *detonation*: the most comprehensive illustration of all the dynamic effects of combustion, exposed here by a phenomenological account of the development and structure of the wave.

The topics of ignition and explosion are presented with primary emphasis on their analytical features, in particular, the nonlinear mechanics character whereby the concept of phase space plays a prominent role in revealing their dynamic properties. The analysis of turbulent flames leads to a novel interpretation of the propagation of combustion waves in terms of what can be aptly called the aerodynamics of flames. The description of the development and structure of detonation waves provides a comprehensive illustration of all the dynamic effects of combustion presented here.

It should be noted that the subject of this paper has been presented in a preliminary form as an invited general lecture at the Ninth U.S. Congress of Applied Mechanics and an abbreviated version published in the Proceedings of the Congress (Oppenheim 1982). The major object of this paper is to provide a unified treatment for the entire field of combustion dynamics, of which a good deal has been presented before in a great number of relatively unrelated publications. In doing this, however, a number of novel interpretations have been revealed.

1. Ignition

The process of ignition, as defined in the Introduction, was commonly referred to in the literature as spontaneous or self-ignition. The fundamental problem was formulated first by Van't Hoff (1896), and the classical solution provided by Semenov (1935), who subsequently expanded this subject by his extensive studies of the chain reaction theory (Semenov 1943;

1944*a*, *b*; 1958; 1959). Since in this connection he concentrated primarily on the chemical kinetic aspects, the effects of diffusion and conduction were disregarded.

Thereupon, following the contributions of Frank-Kamenetskii (1969), an impressive amount of effort was spent on study of the influence of transport phenomena on ignition, whereby the temperature and concentration gradients neglected by Semenov played the essential role (see, for example, Hicks 1954; Gray & Lee 1967; Liñan & Williams 1970; Merzhanov & Averson 1971; Kindelan & Williams 1975; Zeldovich *et al.* 1980). This was associated primarily with interest in the evolution of the so-called 'hot-spot ignition' in condensed explosives. In such circumstances, the geometry of the system became of critical importance, as lucidly exposed by Boddington *et al.* (1971). Most of the subsequent studies on gaseous ignition followed the same trend (see, for example, Kassoy & Poland 1980, 1981; Poland *et al.* 1982; as well as the recent paper of Clarke *et al.* 1984.)

In contrast to these studies, careful consideration of chemical kinetic effects, with transport processes taken into account only as a loss to the surroundings rather than being involved in the evolution of the process, led to the establishment of deterministic thermochemical criteria. This was brought out first by Gray & Yang (1965), Yang & Gray (1967) with relevance to photo-ignition. More recently, a similar approach has been followed by Guirguis *et al.* (1981) in a particular application to ignition of methane–air mixtures. The proper way to look on this method of approach stems from the realization that the problem in its entirety is specified in terms of partial differential equations where the exothermic effects are expressed by source terms. Thus, to emphasize these effects, one treats the governing equations in two fractional steps, the first dealing with sources and the second with transport phenomena. The first step is specified in terms of ordinary differential equations where time is the only independent variable. It is this step only and its consequences that are considered here in detail.

To cast the exposition into a concise form, it is convenient to think of the source term as an expression of the dynamic properties of an *exothermic centre* (a more appropriate name than the 'hot spot'), consisting of a thermodynamically closed *kernel* where chemical reaction takes place, and non-reactive *surroundings* which absorb the work of expansion and serve as a heat sink. This is illustrated in figure 1. Displayed on the left are the time profiles of the evolution of exothermic energy Q in the kernel, and its rate, the exothermic power $\dot{Q}$, normalized with respect to their maxima. Shown on the right is the time–space profile of the boundary of the kernel and the characteristics of the flow field in the surroundings generated by its expansion.

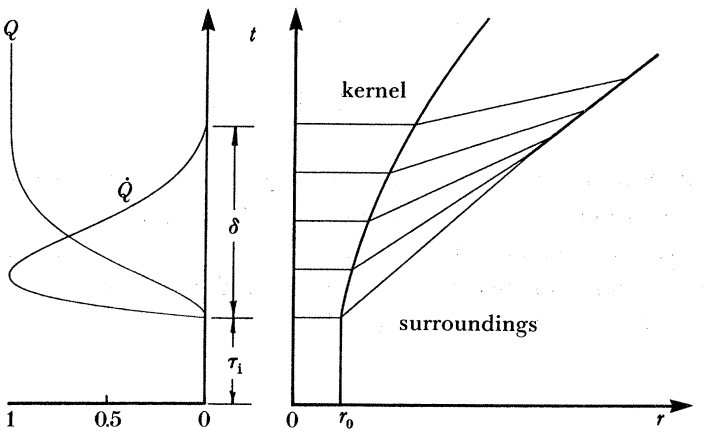

FIGURE 1. Salient features of an exothermic centre.

The kernel, as indicated in figure 1, is devoid of any gradients so that its chemical reaction is spatially homogeneous and, thus, temporally coherent, while the process of compression it induces in the surroundings is a spatially inhomogeneous blast wave. The behaviour of this system can be described in a conventional manner by the chemical rate equations that specify the transformation of molecular species taking place in the kernel, combined with the energy conservation equation that includes heat losses to surroundings and the work of compression. The evaluation of the last term involves consideration of the equation of motion for the compression wave generated by the expanding kernel. In what follows, the application of these three equations to the exothermic centre are considered in turn.

1.1. *Chemical rate equations*

The chemical process is activated by a chain reaction mechanism. Its kinetic scheme consists accordingly of a set of elementary steps, each expressing, in principle, a single collisional event. Thus, for I chemical species, X_i, one has a set of J elementary steps, each of the form

$$\sum_{i=1}^{I} [\nu_{fji} X_i] \underset{k_{rj}}{\overset{k_{fj}}{\rightleftharpoons}} \sum_{i=1}^{I} [\nu_{rji} X_i], \tag{1.1}$$

where ν_{lji} $(l = f, r)$ are the stoichiometric coefficients,

$$k_{lj} = A_{lj}\, T_v^{n_{lj}} \exp(-E_{lj}/RT) \tag{1.2}$$

is the so-called rate constant expressed in a modified Arrhenius form, A_{lj}, n_{lj}, E_{lj} and R being essentially constant, while T is the absolute temperature.

The rate of the generation of any constituent species per unit mass, specifying the *chemical source* of the kernel, is expressed then as:

$$\mathrm{d}(X_i)/\mathrm{d}t = r_{ri} - r_{fi}, \tag{1.3}$$

where

$$r_{li} = \sum_{j=1}^{J} \left[v^{1-m_{lj}} k_{lj} \prod_{i=1}^{I} (X_i)^{\nu_{lji}} \right]. \tag{1.4}$$

In the above

$$m_{lj} \equiv \sum_{i=1}^{I} \nu_{lji},$$

while

$$v = ZRT/p, \tag{1.5}$$

whereas

$$\boldsymbol{Z} \equiv \{(X_i) : i = 1, I\},$$

and

$$Z \equiv \sum_{i=1}^{I} (X_i).$$

Here, parentheses denote species concentrations expressed in moles per unit mass (whence the mass fraction of a constituent species is $Y_i = M_i(X_i)$, M_i being its molar mass). Symbols v and p denote, respectively, the specific volume and pressure of the reactive mixture in the kernel, the relation between them expressed by (1.5) being predicated, of course, by the assumption that each constituent behaves thermodynamically as a perfect gas.

1.2. *Energy equation*

The change of state taking place in the kernel over a differential step in time is displayed on the Le Chatelier diagram, figure 2. In terms of the quantities indicated there, the energy equation per unit mass of the reacting mixture in the kernel is expressed as

$$\mathrm{d}q_e = \mathrm{d}e + p\,\mathrm{d}v + \mathrm{d}q_s, \tag{1.6}$$

where

$$\mathrm{d}q_e \equiv \sum_{i=1}^{I} [e_i(T, X_i) - e_i(T, X_i + \mathrm{d}X_i)]$$

is the exothermic energy evolved in the kernel,

$$\mathrm{d}e \equiv \sum_{i=1}^{I} c_{vi}(T, X_i + \mathrm{d}X_i)\,\mathrm{d}T = \hat{c}_v\,\mathrm{d}T, \tag{1.7}$$

where

$$\hat{c}_v \equiv \sum_{i=1}^{I} \tilde{c}_{vi}(T)\,(X_i),$$

is the increase in the sensible internal energy of the kernel; $p\,\mathrm{d}v$ is the work of its expansion, and $\mathrm{d}q_s$ its heat loss to the surroundings, c_v expressing the specific heat at constant volume, while the hat indicates that its value is expressed per mole of a constituent.

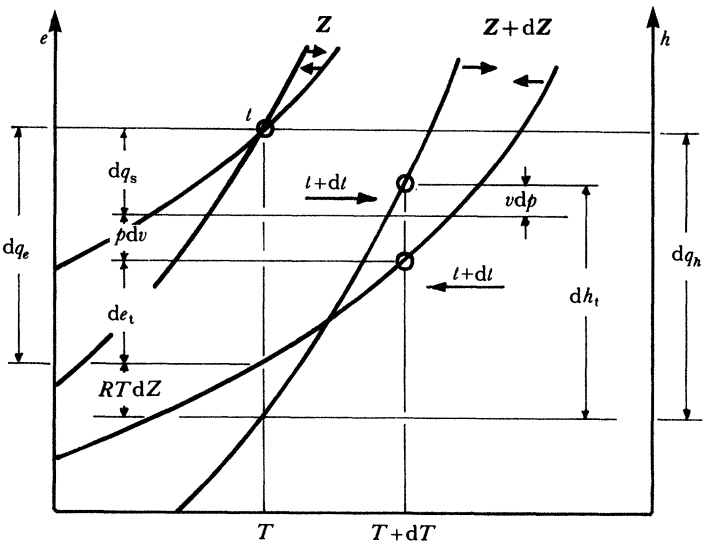

FIGURE 2. The Le Chatelier diagram of the thermodynamic process that takes place in the kernel of an exothermic centre over a differential time step.

By noting that

$$e_i(T, X_i + \mathrm{d}X_i) = e_i(T, X_i) + \tilde{e}_i(T)\,\mathrm{d}(X_i), \tag{1.8}$$

(1.6) becomes

$$\sum_{i=1}^{I} \tilde{e}_i(T)\,\mathrm{d}(X_i) + \hat{c}_v\,\mathrm{d}T + p\,\mathrm{d}v + \mathrm{d}q_s = 0. \tag{1.9}$$

Now, according to (1.5),

$$p\,\mathrm{d}v = RT\,\mathrm{d}Z + RZ\,\mathrm{d}T - v\,\mathrm{d}p, \tag{1.10}$$

while, taking into account the definition of Z,

$$\tilde{e}_i(T)\,\mathrm{d}(X_i)+RT\,\mathrm{d}(X_i)=\tilde{h}_i(T)\,\mathrm{d}(X_i) \tag{1.11}$$

and

$$\tilde{c}_v(T)\,(X_i)+R(X_i)=\tilde{c}_{pi}(T)\,(X_i) \tag{1.12}$$

where h is the enthalpy and c_p the specific heat at constant pressure.

Thus, (1.9) becomes

$$\sum_{i=1}^{I}\tilde{h}_i(T)\,\mathrm{d}(X_i)+\hat{c}_p\,\mathrm{d}T-v\,\mathrm{d}p+\mathrm{d}q_\mathrm{s}=0, \tag{1.13}$$

where, as for $\hat{c}_v$,

$$\hat{c}_p\equiv\sum_{i=1}^{I}\tilde{c}_{pi}(T)\,(X_i)$$

and the energy balance is expressed equivalently to (1.6) as

$$\mathrm{d}q_h=\mathrm{d}h-v\,\mathrm{d}p+\mathrm{d}q_\mathrm{s}. \tag{1.14}$$

This is indicated on the right side of figure 2.

Consequently, the action of the thermal source created by the reacting mixture in the kernel, supplementing (1.3) in the description of its dynamic behaviour, takes the following form:

$$\mathrm{d}T/\mathrm{d}t=\dot{\boldsymbol{Q}}+\dot{\boldsymbol{P}}-\dot{\boldsymbol{L}}, \tag{1.15}$$

where the first term

$$\dot{\boldsymbol{Q}}\equiv\frac{1}{\hat{c}_p}\sum_{i=1}^{I}\left[-\tilde{h}_i(T)\,\frac{\mathrm{d}(X_i)}{\mathrm{d}t}\right]$$

expresses the exothermicity rate, the second term

$$\dot{\boldsymbol{P}}\equiv\frac{v}{\hat{c}_p}\,\frac{\mathrm{d}p}{\mathrm{d}t}$$

represents the compression rate, while the third term

$$\dot{\boldsymbol{L}}\equiv\frac{1}{\hat{c}_p}\,\frac{\mathrm{d}q_\mathrm{s}}{\mathrm{d}t}$$

is the loss rate. Each of these terms is essentially a positive quantity.

As evident from (1.15), there are two limiting cases of specific interest:

(*a*) mild ignition: a constant pressure process when the compression rate $\dot{\boldsymbol{P}}$ vanishes;

(*b*) strong ignition: an adiabatic runaway process when the loss rate $\dot{\boldsymbol{L}}$ vanishes.

1.3. *Mild ignition; thermal relaxation*

In this case there is no interaction between exothermic centres so that the whole system behaves as any of its elementary components. The problem is, therefore, completely defined in terms of a set of $I+1$ autonomous equations (1.3) and (1.15) with $\dot{\boldsymbol{P}}=0$, subject to initial conditions specified by a given temperature T_0 and mass fraction of chemical species Y_{i0} The solution is obtained by computations with proper care to handle the 'stiffness' of the rate equations (1.3) as, for example, by the multi-step technique of Gear (1971).

As it will be seen presently, the results turn out to be relatively insensitive to the magnitude of the loss rate. Consequently, it is convenient to express this term simply as

$$\dot{\boldsymbol{L}}=(T-T_\mathrm{s})/\tau_\mathrm{t},$$

where the subscript s denotes the surroundings,

$$\tau_t \equiv l\hat{c}_p/vH$$

is the thermal relaxation time, l being the volume to area ratio of the kernel, and

$$H \equiv [l/v(T-T_s)]\,\mathrm{d}q_s/\mathrm{d}t$$

is its overall heat transfer coefficient. Treating the heat loss this way is tantamount to assuming that the effect of internal conduction is negligible in comparison with that of external convection, as clearly expressed by Boddington *et al.* (1971) in their equations (3.1) and (3.2): a concept fully consistent with our model.

One thus obtains information on the time resolved concentration and temperature profiles, as exemplified by figure 3 (Carter *et al.* 1985). It presents a solution derived for the case of a stoichiometric hydrogen–air mixture, $H_2+0.5O_2+1.88N_2$, with chemical kinetics prescribed by table 1, that has been initially at a pressure of 6 atm† and a temperature of either 775 K (represented by continuous lines) or 774 K (broken lines), while the thermal relaxation time τ_t is 1 s. As evident from the figure, the two initial temperatures bracket a critical threshold for ignition, below which the process decays to extinction. One should note that the existence of losses are, for this purpose, essential, since in their absence, i.e. for $\tau_t = \infty$, extinction cannot occur: a consequence of the Arrhenius law according to which the chemical source term governing the exothermicity rate is positive at all temperatures.

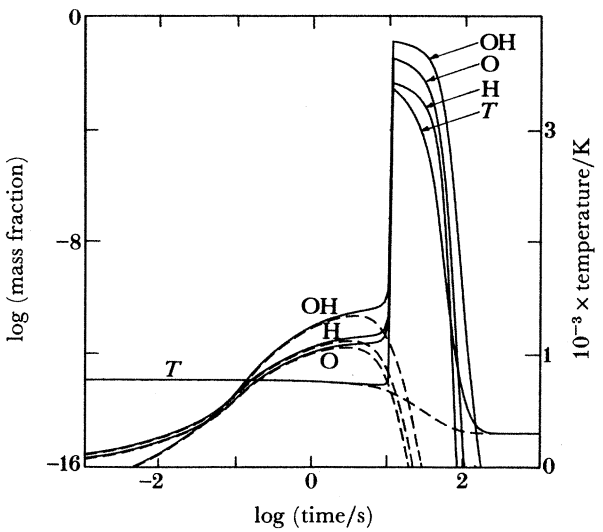

FIGURE 3. Temperature and radical concentration profiles for a stoichiometric hydrogen–oxygen mixture initially at a pressure of 6 atm and temperatures of 775 K (continuous lines) and 774 K (broken lines) while the thermal relaxation time is 1 s.

Figure 4 presents critical ignition temperatures evaluated in this manner over a range of initial pressures from 10^{-4} to 10 atm, in comparison with the experimentally established thermal ignition limits, usually classically referred to in the literature as 'explosion limits' (Lewis & Von Elbe 1961). The computed curves, one corresponding to $\tau_t = 1$ s and the other to $\tau_t = 30$ s, are in a remarkably close agreement with the classical limits over all their three

† 1 atm = 101 325 Pa.

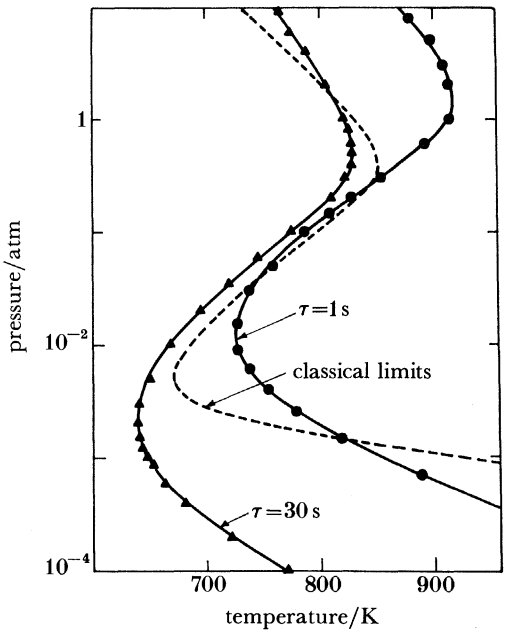

FIGURE 4. Thermal ignition limits for the hydrogen–oxygen system.

TABLE 1. KINETIC MECHANISM FOR THE H_2–O_2 SYSTEM AND PARAMETERS OF REACTION RATE CONSTANTS[a]

($k = AT^n \exp(-E/RT)$, where k is in (cm³/mole)/s or (cm³/mole)²/s, T and K, and E in kcal/mole[b].)

	reaction	A	n	E	remarks
1.	$OH+O \rightarrow O_2+H$	0.18×10^{14}	0	0	—
2.	$O+H_2 \rightarrow OH+H$	0.15×10^{8}	2	7.55	—
3.	$OH+H_2 \rightarrow H_2O+H$	0.18×10^{9}	1.6	3.3	—
4.	$OH+OH \rightarrow H_2O+O$	0.15×10^{10}	1.14	0	—
5.	$H+H+M \rightarrow H_2+M^c$	0.64×10^{18}	−1	0	M = Ar $k_5(M=H_2)=0$
6.	$H+H+H_2 \rightarrow H_2+H_2$	0.97×10^{17}	−0.6	0	—
7.	$H+OH+M \rightarrow H_2O+M^c$	0.14×10^{24}	−2	0	—
8.	$H+O_2+M \rightarrow HO_2+M^c$	0.7×10^{18}	−0.8	0	M = Ar
9.	$O+O+M \rightarrow O_2+M^c$	0.1×10^{18}	−1	0	M = Ar
10.	$H+HO_2 \rightarrow OH+OH$	0.15×10^{15}	0	1	—
11.	$H+HO_2 \rightarrow H_2+O_2$	0.25×10^{14}	0	0.69	—
12.	$O+HO_2 \rightarrow OH+O_2$	0.2×10^{14}	0	0	—
13.	$OH+HO_2 \rightarrow H_2O+O_2$	0.2×10^{14}	0	0	—
14.	$HO_2+HO_2 \rightarrow H_2O_2+O_2$	0.2×10^{13}	0	0	—
15.	$OH+OH+M \rightarrow H_2O_2+M^c$	0.13×10^{23}	−2	0	$M=O_2$
16.	$H+H_2O_2 \rightarrow H_2+HO_2$	0.17×10^{13}	0	3.75	—
17.	$O+H_2O_2 \rightarrow OH+HO_2$	0.28×10^{14}	0	6.4	—
18.	$OH+H_2O_2 \rightarrow H_2O+HO_2$	0.7×10^{13}	0	1.43	—
19.	$H+H_2O_2 \rightarrow H_2O+OH$	0.1×10^{14}	0	3.58	—

[a] Based on the compilations of Baulch *et al.* (1972), verified by Dixon-Lewis (1979), selected by the sensitivity analysis of Dougherty & Rabitz (1980), and recommended by Warnatz (1984).

[b] 1 cal = 4.186 800 J.

[c] Relative ter-molecular reaction efficiencies (multiplicators of A) are, respectively $\epsilon(H)=1$: $\epsilon(O_2)=0.4$, $\epsilon(H_2O)=6.5$, and $\epsilon(Ar)=0.35$.

PHILOSOPHICAL TRANSACTIONS OF THE ROYAL SOCIETY A MATHEMATICAL, PHYSICAL & ENGINEERING SCIENCES

segments: the so-called 'first explosion limit' at low pressures considered in classical literature to be caused by quenching at the wall, the 'second explosion limit' at intermediate pressures credited to the onset of chain branching, and the 'third explosion limit', at high pressures ascribed to the influence of that conduction. The ability to account for all three on the basis of a single comprehensive theory seems to be a noteworthy unification. It is, moreover, of significance to observe that, although the existence of self-ignition limits depends crucially on a finite value of the relaxation time, the magnitude of this time is relatively unimportant, the actual pressures and temperatures at which the limits occur being remarkably insensitive to it, especially along the pivoted second explosion limit.

The most informative way to display sets of solutions for the problem of ignition is in the form of integral curves on an $(I+1)$-dimensional phase space: a space whose coordinates are the concentrations of all of the chemical species participating in the reaction, and the temperature. Examples of such solutions are presented in figure 5, the projection of integral curves on the plane of the hydrogen atom concentration and the temperature. They were determined for a stoichiometric hydrogen–air mixture initially at a pressure of $p = 6$ atm while the thermal relaxation time τ_t equals 1 s. Families of integral curves depicted there correspond to two sets of initial temperatures and two cases of initial concentration of radicals, namely

(a) zero, i.e. $(Y_H)_0 = (Y_O)_0 = (Y_O)_0 = 0$ (the thermal case);

(b) finite, i.e. $(Y_H)_0 = 10^{-3}$ while $(Y_{OH})_0 = (Y_O)_0 = 0$ (the thermochemical case).

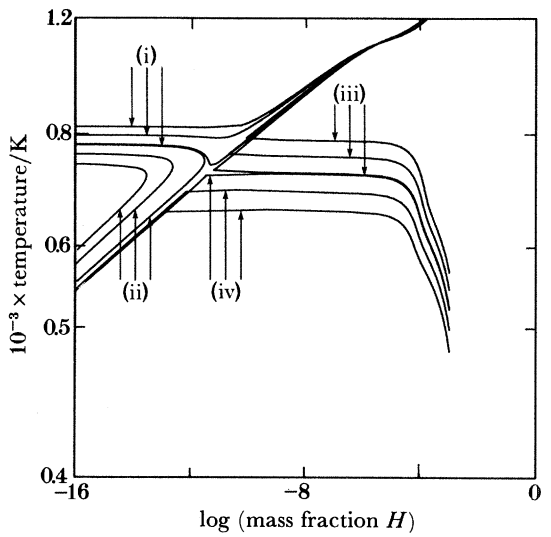

FIGURE 5. Integral curves of ignition for a stoichiometric hydrogen–oxygen mixture at a pressure of 6 atm, while the thermal relaxation time is 1 s.

There are four families: (i) ignition for case (a), (ii) extinction for case (a), (iii) ignition for case (b), and (iv) extinction for case (b). The division between ignition and extinction is a separator, its initial point specifying the critical threshold for ignition: the ignition temperature. The division between families of case (a) and case (b) is an attractor: a surface in the phase space which all the integral curves tend to approach, specifying a critical composition of a radical pool attained by the reacting system at a critical intermediate stage of the process.

For a chemical kinetic scheme involving only one radical, a graph such as figure 5, instead

of representing a projection of integral curves existing in a multi-dimensional phase space, acquires the role of a phase plane where the intersection between the separator and the attractor is a saddle point singularity. It is this plane that has been elucidated by Gray & Yang (1965).

The feature of most practical importance revealed in the phase space is that the critical threshold for ignition is significantly lower in case (*b*) than in case (*a*), as clearly manifested in figure 5. Thus, the attractor represents not only the envelope of all the integral curves for case (*a*), delineating the maximum concentration the radicals can reach in the course of thermal ignition, but it also specifies the minimum concentration of radicals that is required to exert a significant influence on the ignition threshold, a feature leading to the attainment of appreciably lower ignition temperatures.

1.4. *Strong ignition kernel; equation of motion*

As illustrated in figure 1, the dynamic effects of ignition are manifested by the compression wave generated by the expanding kernel in the surroundings. The limiting case of strong ignition occurs when the last term of (1.15) ($\dot{\boldsymbol{L}}$) vanishes. In this case one can admit the possiblity of perfect interaction between exothermic centres so that they are fully coherent. The whole system behaves then as a single elementary component: the same outcome as in the previous case but for a different reason. However, unlike the former, performance characteristics of a strong ignition kernel depend on its size.

While a good deal of experimental evidence of this case has been obtained in the course of knock and detonation studies (see, for example, Sokolik 1960; Saytzev & Soloukhin 1962; Voyevodsky & Soloukhin 1965; Meyer & Oppenheim 1971 *a*, *b*), there is also ample knowledge available on its theoretical background (see, for example, Van Tiggelen 1969; Borisov 1974; Oppenheim *et al.* 1974, 1975). In this respect, the most informative computations were done by Zajac & Oppenheim (1971) and by Cohen *et al.* (1975 *a*) as well as by Cohen & Oppenheim (1975), in which the compression of the surroundings was treated as a blast wave.

Expansions of exothermic kernels with initial radius of $r_0 = 1$ mm, evaluated in this way for a stoichiometric hydrogen–oxygen mixture at initial conditions of $T_0 = 1336$ K and $p_0 = 3.236$ atm (while the surroundings are considered as a perfect gas with specific heat ratio $\gamma = 1.14$ and local velocity of sound $a_0 = 1.02$ km s^{-1}), are displayed in figure 6 for the planar, axial, and point symmetrical case, corresponding to $j = 0$, 1, and 2, respectively. Depicted there by broken lines are the asymptotic limits expressed by the volumetric expansion at constant pressure, evaluated by the use of (1.5), its square and cube roots, respectively.

The concomitant exothermic processes occurring in the kernel are presented on the pressure-specific volume diagram, figure 7, in comparison with conventional processes including a Chapman–Jouguet deflagration. As clearly evident from there, the process of an exothermic kernel is distinguished from the others by the unique feature of progressing, at its evolutionary stage, along a path of a simultaneously increasing pressure and specific volume. This has a significant effect on the power density of the kernel, as shown in figure 8, where the exothermic pulses on the phase plane of power and energy are presented. For this purpose, the latter is expressed in terms of the Hugoniot parameter $\Psi \equiv (P+\beta)(V-\beta)$ where $P \equiv p_k/p_0$, $V \equiv v_k/v_0$, $\beta \equiv (\Gamma-1)/(\Gamma+1)$, while $\Gamma \equiv -(\partial \ln p/\partial \ln v)_\phi$ is the isentropic index, ϕ denoting the entropy. It should be noted that for a perfect gas $\Gamma = \gamma \equiv c_p/c_v$.

The dynamic nature of the system can be best described on the basis of a simplifying assumption suggested by figure 1: namely that the effects of the blast wave at the interface between the kernel and the surroundings can be expressed in terms of a simple wave.

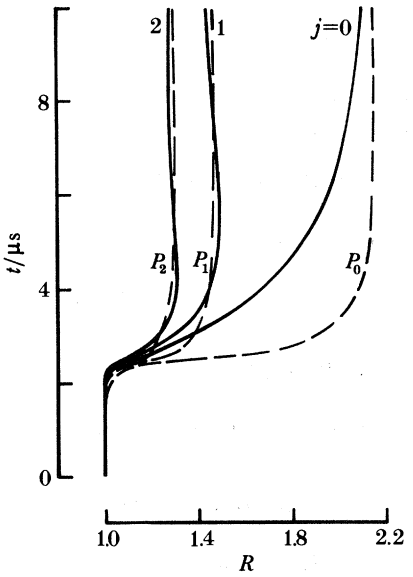

FIGURE 6. Time–space trajectories of the interface of a strong ignition kernel in a stoichiometric hydrogen–oxygen mixture initially at $T_0 = 1336$ K and $p_0 = 3.236$ atm, while the initial radius of the kernel $r_0 = 1$ mm for planar ($j = 0$), cylindrical ($j = 1$, and spherical ($j = 2$) geometry (Cohen *et al.* 1975). Broken lines represent the corresponding limits in the variation of specific volume P_0, its square root P_1, and cube root, P_2.

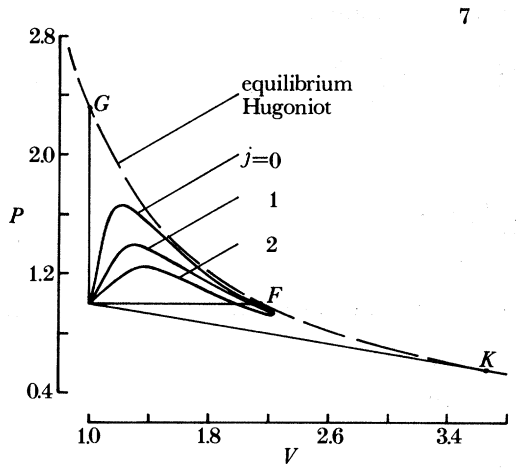

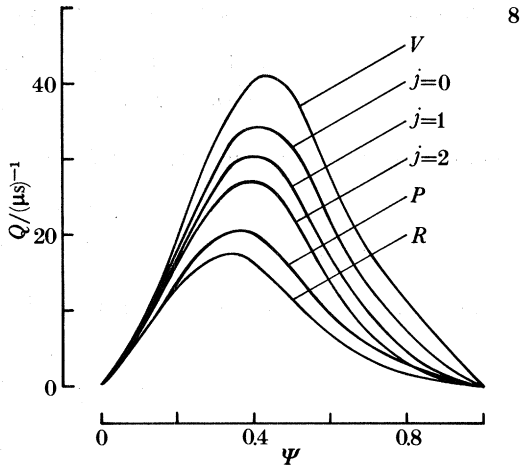

FIGURE 7. Pressure-specific volume diagram of the paths of exothermic processes that take place in the kernels of figure 6 (Cohen *et al.* 1975).

FIGURE 8. Exothermic power pulses of processes displayed in figure 7 (Cohen *et al.* 1975).

The analysis can be thus based on the equation of motion across a characteristic (see, for example, Oppenheim 1972)

$$a\,\mathrm{d}u - v\,\mathrm{d}p = 0, \tag{1.16}$$

where u is the particle velocity, and

$$a \equiv -v(\partial p/\partial v)^{\frac{1}{2}} = (\Gamma p v))^{\frac{1}{2}} \tag{1.17}$$

is the local velocity of sound, the last expression having been obtained by virtue of the definition of Γ given above.

Equations (1.16) and (1.17) yield

$$\mathrm{d}p/\mathrm{d}u = \Gamma p/a. \tag{1.18}$$

In terms of normalized parameters defined above and $U \equiv u/a_0$, and by taking into account (1.17) and the definition of Γ, this becomes

$$\mathrm{d}P/\mathrm{d}U = \Gamma P^{(\Gamma+1)/2\Gamma}, \tag{1.19}$$

so that by straightforward integration, subject to the initial condition $P = 1$ at $U = 0$,

$$U = [2/(\Gamma-1)]\,F(P), \tag{1.20}$$

where

$$F(P) \equiv P^{(\Gamma-1)/2\Gamma} - 1.$$

Particle velocity at the interface is in turn directly related to volumetric expansion of the kernel, that is

$$U \equiv \mathrm{d}R/\mathrm{d}\eta = \kappa V^{\kappa} W, \tag{1.21}$$

where V is the specific volume ratio (v_k/v_0), while

$$W \equiv \mathrm{d}\ln V/\mathrm{d}\eta$$

and $R \equiv r_k/r_0$, $\eta \equiv a_0\, t/r_0$, the index κ taking values 1, $\frac{1}{2}$, or $\frac{1}{3}$ for planar, cylindrical, or spherical geometry of the kernel, respectively.

Equation (1.19), (1.20) and (1.21) yield the following relations:

$$\frac{\mathrm{d}U}{\mathrm{d}R} \equiv \frac{1}{U}\frac{\mathrm{d}^2R}{\mathrm{d}\eta} \equiv \frac{\mathrm{d}\ln U}{\mathrm{d}\eta} = \frac{\mathrm{d}\ln F(P)}{\mathrm{d}\eta} = \frac{\mathrm{d}\ln W}{\mathrm{d}\eta} + \kappa W, \tag{1.22}$$

whereas from the definition of $F(P)$ it follows that

$$\frac{\mathrm{d}\ln P}{\mathrm{d}\eta} = \frac{2\Gamma}{\Gamma-1}\frac{\mathrm{d}\ln[F(P)+1]}{\mathrm{d}\eta}. \tag{1.23}$$

Hence, taking into account the equation of state (1.5), the compression rate of (1.15) becomes

$$\dot{P} = \frac{2}{\Gamma-1}\frac{a_0^3}{\hat{c}_p r_0} Z\Theta \frac{\mathrm{d}\ln[F(P)+1]}{\mathrm{d}\eta}, \tag{1.24}$$

where

$$\Theta \equiv T_k/T_0.$$

With the above, (1.15) brings out the runaway nature of the exothermic centre. The deposition of energy in the kernel, due to the exothermicity of the reaction, causes its volumetric expansion which, by virtue of the positive compression rate, contributes further to the increase in its temperature rise that, in turn, enhances the exothermicity rate. This is abetted by the drastic difference between the paths of the compression process in the kernel and in its surroundings. One, being associated with simultaneously increasing pressure and specific volume, crosses the lines of constant temperature at a much larger angle than the other, practically coinciding with a line of constant entropy. Thus once the exothermic reaction starts in the kernel as a consequence of its higher initial temperature than that in the surroundings, the temperature difference on the two sides of its interface with the surroundings becomes subsequently augmented. The most interesting aspect of this is the fact that loss of energy due

to the work done by compressing the surroundings contributes toward the acceleration of the process. This elucidates the essential elementary cause of such well known intrinsic instability phenomena in combustion as knock in internal combustion engines (see, for example, Sokolik 1960) and the 'explosion in the explosion' at the onset of detonation (Urtiew & Oppenheim 1966).

1.5. *Strong ignition limit*

As is evident from (1.15), the dynamic effects of ignition depend primarily on the magnitude of the specific power pulse, expressed by the exothermicity rate $\dot{Q}(t)$. The pulse amplitude can be controlled by diluting the reactive mixture with an inert additive, or by adjusting its initial pressure and temperature. These effects can be studied most conveniently in a shock tube, by using the reflected wave technique.

Optical observations reveal that in such circumstances mild ignition is manifested at its outset by the formation of flame kernels, usually developed in corner eddies which are generated as a consequence of the interaction of the reflected wave with the boundary layer created by the incident shock. This is illustrated in figure 9, plate 1, which presents a cinematographic sequence of laser schlieren photographs of ignition in an iso-octane–oxygen mixture at a pressure of 6 atm and a temperature of 1300 K, taken at a frequency of 500 kHz.

Strong ignition, on the other hand, is distinguished by the fact that at first a front of a blast wave is formed by the deposition of exothermic energy in the reacting medium without any prior evidence of flame kernels, as displayed in figure 10 which was obtained for the same pressure as figure 9 but for a temperature of 1400 K. Here, in contrast to the elementary strong ignition kernel exposed in the previous section, the surroundings undergo and exothermic process, a circumstance that can be taken into account by considering it to be an infinite set of consecutively initiated elementary strong exothermic kernels (see, for example, Oppenheim *et al.* 1975*a*, *b*).

The strong ignition limit is the line of demarcation between the régimes of mild and strong ignition on the plane of initial temperatures and pressures. It has been identified first by Saytzev & Soloukhin (1962) and according to the early theory proposed by Voyevodsky & Soloukhin (1965), it has been considered as an extension of the 'second explosion limit' into the 'explosion' régime.

An experimentally determined strong ignition limit for a stoichiometric hydrogen–oxygen mixture is presented in figure 11 (Meyer & Oppenheim 1971*a*). As indicated there, instead of appearing as an extension of the second limit, it coincides most closely with a locus of the condition $(\partial\tau_i/\partial T)_p = \text{const.}$ where τ_i is the chemical induction time, specified in figure 1. This experimental observation can be rationalized by the following argument (Meyer & Oppenheim 1971*b*).

Consider a set of N exothermic kernels per unit mass of the reacting mixture, developing under the influence of a Gaussian temperature distribution. Then

$$\frac{\mathrm{d}\ln N}{\mathrm{d}T} = \frac{1}{(2\pi)^{\frac{1}{2}}\sigma}\exp\left[-\frac{1}{2}\left(\frac{T-T_m}{\sigma}\right)^2\right], \tag{1.25}$$

where σ is the standard deviation and subscript m denotes the mean.

In view of the exponential dependence of the induction time on the reciprocal of the

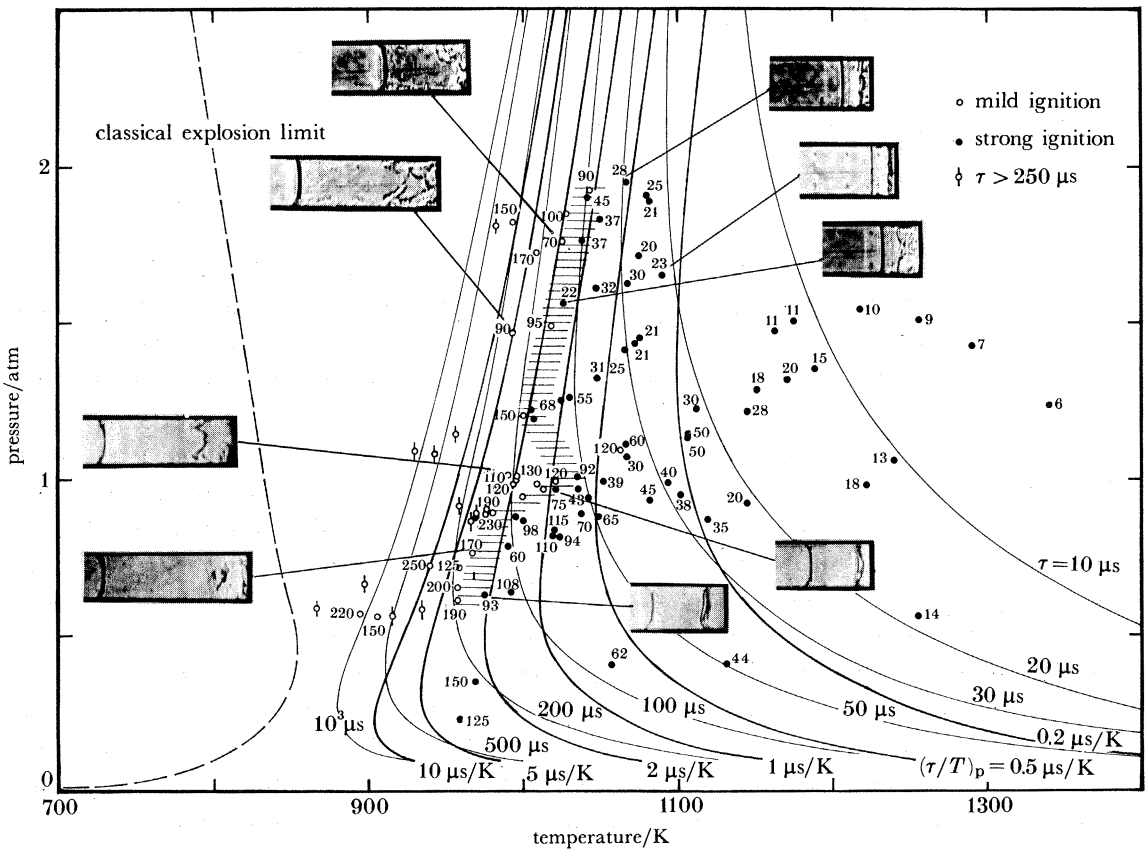

FIGURE 11. Strong ignition limit – the demarcation between mild and strong ignitions – for the stoichiometric hydrogen–oxygen system (Meyer & Oppenheim 1971*a*).

temperature, implied by the Arrhenius relation, the corresponding distribution of this time at constant pressure can be expressed by a Taylor series truncated at the linear term, i.e.

$$\tau_i = \tau_m - (\partial \tau_i / \partial T)_p \, (T - T_m). \tag{1.26}$$

Thus, (1.25) becomes

$$\frac{\mathrm{d} \ln N}{\mathrm{d}\tau_i} = \frac{1}{(2\pi)^{\frac{1}{2}} \omega} \exp\left[-\frac{1}{2} \left(\frac{\tau_i - \tau_m}{\omega} \right)^2 \right], \tag{1.27}$$

where $\omega \equiv -(\partial \tau_i / \partial T)_p \, \sigma$.

Noting that for the purpose at hand it should be quite sufficient to consider the case of an average evolution of exothermic energy as a linear function of time, the power pulse of the kernel is a square wave extending over a time interval δ with amplitude equal to a uniform rate of the deposition of the specific exothermic energy, $q(\delta)$. In the case of non-uniform temperature distribution the specific exothermic power at a given instant of time t is obtained from the contribution of exothermic kernels whose induction times lie within the interval $\tau_{i1} = t - \delta$ and $\tau_{i2} = t$. Thus, by integrating (1.29) from τ_{i1} to τ_{i2} while the specific exothermic energy and time are normalized, the former with respect to its total value for the reacting mixture,

$Q \equiv q(t)/q(\delta)$, and the latter with respect to the pulse width $\theta \equiv t/\delta$, one obtains a non-dimensional expression for the specific exothermic power

$$\dot{Q} \equiv \frac{\mathrm{d}Q}{\mathrm{d}\theta} = \frac{N(\delta)}{N} = \frac{1}{2}\left[\mathrm{erf}\left(\frac{\{\theta-\theta_{\mathrm{m}}\}}{(2\pi)^{\frac{1}{2}}}\frac{\delta}{\omega}\right) - \mathrm{erf}\left(\frac{\{\theta-\theta_{\mathrm{m}}-1\}}{(2\pi)^{\frac{1}{2}}}\frac{\delta}{\omega}\right)\right]. \tag{1.28}$$

Equation (1.28) describes, in essence, the dependence of the specific exothermic power pulse on the standard deviation of induction times ω. Its plot is presented in figure 12, where this deviation appears as a parameter expressed as a multiple of the exothermic pulse widths δ. As evident there, all the maxima occur at $\theta_{\mathrm{m}} + \frac{1}{2}$, and (1.30) yields, for this value of θ, the following relation between the decay in peak specific power and the standard deviation in temperature distribution:

$$\dot{Q}_{\max} = \mathrm{erf}\left[-\frac{\delta}{2(2\pi)^{\frac{1}{2}}(\partial\tau_{\mathrm{i}}/\partial T)_p\,\sigma}\right]. \tag{1.29}$$

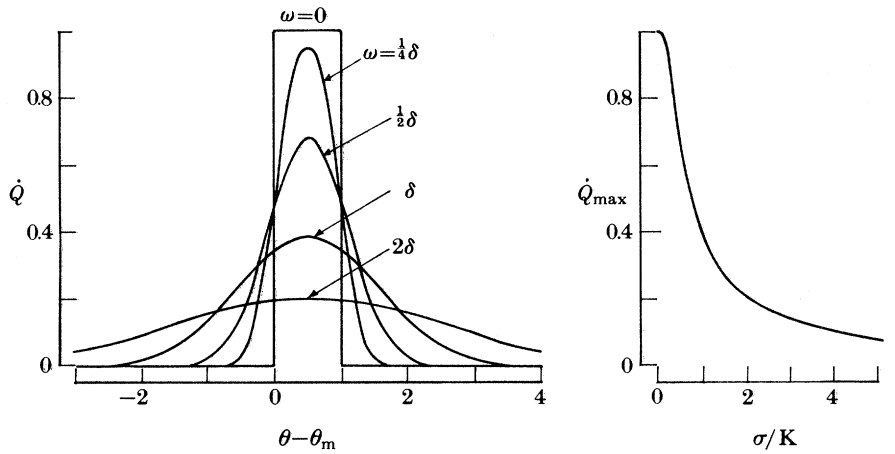

FIGURE 12. Decay of the power pulse for a system of exothermic kernels as a function of the standard deviation in induction times, and the decrease of their maxima as a function of the standard deviation in the temperature distribution for a stoichiometric hydrogen–oxygen mixture (Meyer & Oppenheim 1971*b*).

This demonstrates the commanding influence of the partial derivative of induction time with respect to temperature at constant pressure.

As an example, for the stoichiometric hydrogen–oxygen mixture, as shown in figure 11, at the strong ignition limit one has

$$(\partial\tau_{\mathrm{i}}/\partial T)_p = -2\ \mu\mathrm{s/K},$$

while from the numerical analysis of Cohen *et al.* (1975*a*, *b*, *c*) it appears that the average duration of the power pulse for this mixture at a temperature of order 1000 K is $\delta = 2\mu$s. With these values, (1.29) specifies the decay of the peaks in power pulses displayed on the right side of figure 12.

The result is quite striking. A deviation of only four degrees at a level of 1000 K is associated with a tenfold decrease in peak specific power of an exothermic kernel. It is this remarkable sensitivity to temperature distribution that manifests the critical nature of the strong ignition limit.

Finally, it should be noted that an experimental study of strong ignition limit for hydrocarbons done by Vermeer *et al.* (1972) revealed that, in this case, the limit coincides with a line of a constant $(\partial \ln \tau_i/\partial T)_p$ rather than $(\partial \tau_i/\partial T)_p$, as established by Meyer & Oppenheim (1971 *a*) for hydrogen. On the basis of (1.29), this can be explained by observing that the width of the exothermic power pulse δ is evidently proportional to the induction time τ_i for hydrocarbons, whereas for hydrogen it is relatively invariant.

2. Inflammation

This process is illustrated here by the particular case of a turbulent flame in a combustion tunnel. For clarity, we consider it to take place under the most idealized conditions. The flowing substance is assumed to consist of two imcompressible media: the reactants and the products, differing from each other only by the relative value of specified volumes (or densities), a property manifesting the major effect of the exothermicity of combustion. The transformation from one to the other occurs at the flame front, treated as an infinitesimally thin interface (in accord with the so-called thin flame model) which corresponds to the assumption that the chemical kinetic processes are infinitely fast. The flow field is, moreover, treated as strictly planar. A numerical modelling analysis of this process has been published recently (Ghoniem *et al.* 1982). Its highlights are as follows:

2.1. *Formulation*

With the assumptions specified above, the flow field obeys the continuity and the Navier–Stokes equations expressed, in standard vector notation, respectively as follows:

$$\nabla \cdot \boldsymbol{u} = \epsilon(r_f), \tag{2.1}$$

where $\boldsymbol{u}$ is the velocity vector, while $\boldsymbol{r}_f$ is the coordinate vector of the flame front,

$$\mathrm{D}\boldsymbol{u}/\mathrm{D}t = Re^{-1}\nabla^2\boldsymbol{u} - \nabla p, \tag{2.2}$$

where t is the time coordinate, Re is the Reynolds number at inlet and p is the pressure. In the above, the magnitude of the velocity is normalized with respect to its initial value at inlet, while pressure is non-dimensionalized by the corresponding initial specific momentum of the stream.

The flame front propagates as a consequence of its self-advancement at a normal burning speed S_u in the direction normal to its surface, and by advection due to the flow field where it is situated, that is

$$\mathrm{d}\boldsymbol{r}_f/\mathrm{d}t = S_u \cdot \boldsymbol{n}_f + \boldsymbol{u}, \tag{2.3}$$

where $\boldsymbol{n}_f$ denotes a unit vector normal to the front.

The divergence, which expresses the dynamic effects of combustion, is supported by sources of specific volume whose intensities per unit area (or length in planar flow) of the flame front are

$$u_s = \tfrac{1}{2}(V_f - 1)\, S_u \tag{2.4}$$

where V_f is the specific volume ratio across the flame front. Thus

$$\epsilon(\boldsymbol{r}_f) = u_s \cdot \delta(\boldsymbol{r} - \boldsymbol{r}_f), \tag{2.5}$$

where δ is the Kronecker delta function.

The initial and boundary conditions are, respectively,

$$\boldsymbol{u} = u = 1 \quad \text{at inlet,} \tag{2.6}$$

and

$$\boldsymbol{u} = 0 \quad \text{at all the walls.} \tag{2.7}$$

2.2. *Transformation*

By taking the rotation of each term, (2.2) is transformed into the vortex transport equation

$$\mathrm{D}\xi/\mathrm{D}t = Re^{-1}\nabla^2\xi, \tag{2.8}$$

where

$$\xi \equiv \nabla \times \boldsymbol{u}$$

is the vorticity, while, it should be noted, $\nabla \times \nabla p \equiv 0$.

2.3. *Solution*

The velocity vector field is considered to consist of a solenoidal and a divergence component, i.e.

$$\boldsymbol{u} = \boldsymbol{u}_\xi + \boldsymbol{u}_\epsilon, \tag{2.9}$$

where

$$\nabla \cdot \boldsymbol{u}_\xi = 0 \quad \text{and} \quad \nabla \times \boldsymbol{u}_\xi = \xi, \tag{2.10}$$

subject to boundary conditions

$$\boldsymbol{u}_\xi \cdot \boldsymbol{n} = 0 \quad \text{and} \quad \boldsymbol{u}_\xi \cdot \boldsymbol{s} = 0. \tag{2.11}$$

Here $\boldsymbol{n}$ denotes a unit vector normal to the wall and $\boldsymbol{s}$ a unit vector tangential to the wall, whereas,

$$\nabla \cdot \boldsymbol{u}_\epsilon = \epsilon(\boldsymbol{r}_\mathrm{f}) \quad \text{and} \quad \nabla \times \boldsymbol{u}_\epsilon = 0, \tag{2.12}$$

subject to the boundary condition

$$\boldsymbol{u}_\epsilon \cdot \boldsymbol{n} = 0. \tag{2.13}$$

The solenoidal component is treated by the random vortex method (Chorin 1973, 1978), based on the use of random walk to model the effects of diffusion implied in (2.5), and the divergence component is taken into account by a flame advection and propagation algorithm (Chorin 1980) that combines a simple line interface calculation of Noh & Woodward (1976) with a numerical implementation of the Huygens principle. The structure of the computational algorithms developed on this basis is depicted in figure 13. As evident there, the solenoidal component, which treats the dynamics of the turbulent flow field, derives its primary constituent – the vorticity – from the no-slip boundary condition, (1.9); the divergence component, specified by (2.4) and (2.5), deals with the effects of exothermicity expressed in terms of volume sources.

2.4. *Application*

The practical significance of this method is illustrated by the application to turbulent flow in a combustion tunnel. Specifically, the combustor was a duct of rectangular cross section, 5.1 cm × 17.3 cm, fitted with quartz windows on the shorter sides over a length of 21 cm, and provided with a rear-facing step, 2.54 cm high, at the inlet where a lean propane–air mixture was admitted through a convergent nozzle at a Reynolds number of 2.2×10^4. Extracts of cinematographic schlieren records of the turbulent flame, obtained under such conditions, are

PHILOSOPHICAL TRANSACTIONS OF THE ROYAL SOCIETY A MATHEMATICAL, PHYSICAL & ENGINEERING SCIENCES

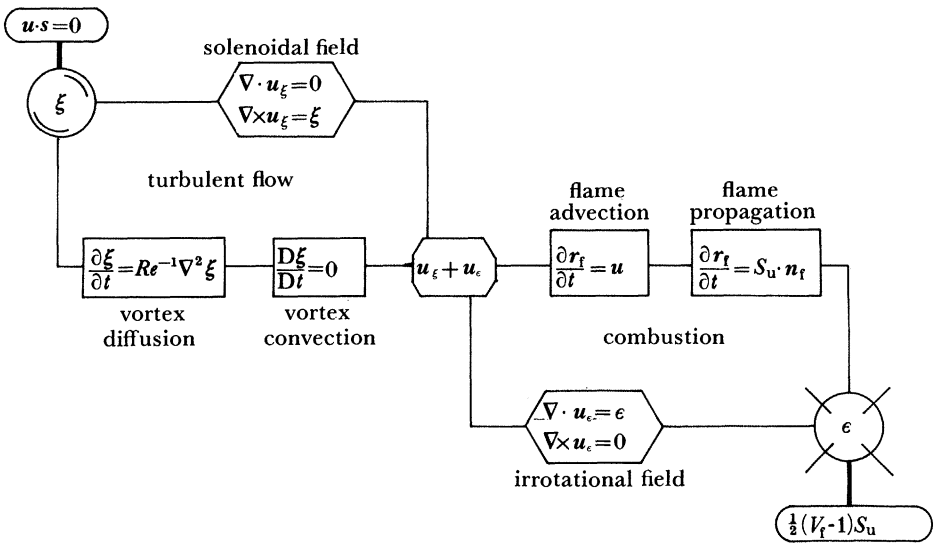

FIGURE 13. Structure of the algorithm for numerical modelling of turbulent combustion by the random vortex method.

presented in figure 14, plate 2. The results of numerical modelling analysis, done recently by Hsiao *et al.* (1985), are displayed in figures 15 and 16. They correspond to the case of $S_u = 0.02$, normalized with respect to the velocity of flow above the step. The resemblances between the experimental records and the results of numerical solution in the shape of the flame depicted in figure 15, as well as in the average axial velocity vector field and the root mean square of its fluctuating component displayed in figure 16, are quite remarkable.

2.5. *Aerodynamics of flames*

The overall similitude between the results of modelling analysis and experimental records demonstrates the capability of the random vortex method to display prominent features of turbulent combustion. Of particular significance to me is the fact that it ushers in a novel treatment of flame motion: the aerodynamics of flames (Oppenheim & Ghoniem 1983). The new concepts formed thereby are, in a nutshell, as follows:

Flames do not propagate only by themselves; they are, as a rule, embedded in a flow field on which they can exert a feedback. Their behaviour should be therefore looked on as a consequence of interaction between the flow field and the exothermic chemical reaction. The flame, at the interface between the relatively inviscid unburnt and burnt gases, behaves as a readily deformable, semi-permeable membrane along which the tangential flow velocity is significantly higher than its orthogonal component, the normal burning speed. Of crucial importance to the dynamic behaviour of the flow system is the considerable growth in the specific volume of the gas crossing the flame front, because of the exothermicity of the combustion process. In such circumstances the fresh mixture can sustain combustion at a relatively small expenditure of its overall mass flow rate. As illustrated in figures 14–16, the obstruction imposed by the aerodynamic body of the burnt medium brings about an acceleration of unburnt gases, providing the flame with a lift that enhances the effect of expansion. All that is associated with large scale eddy motion (the recirculation that helps to

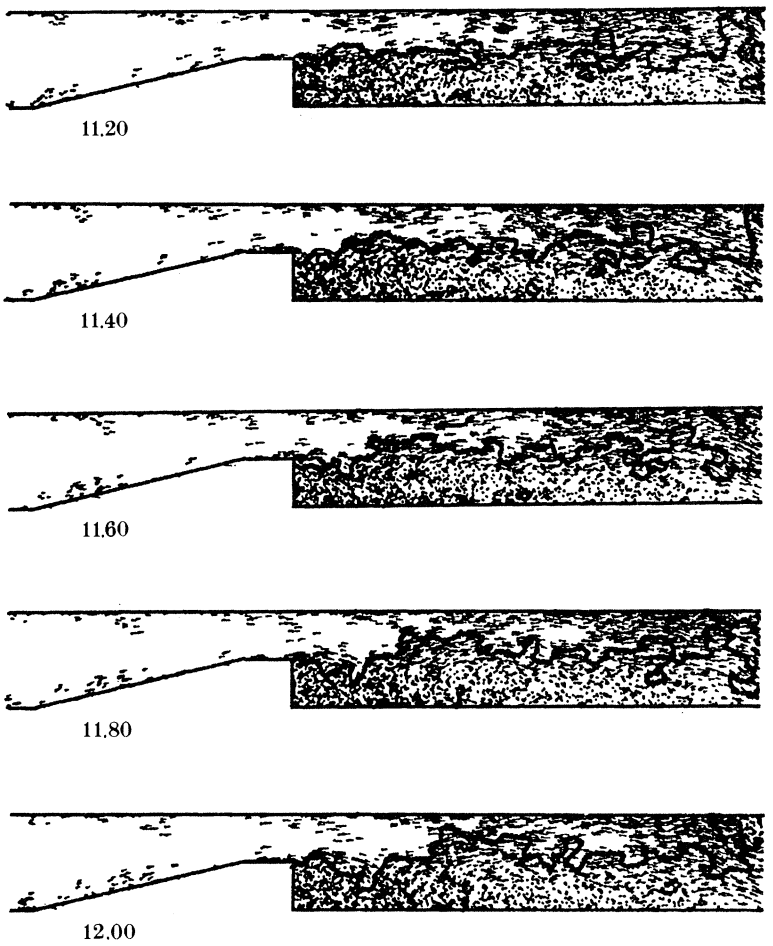

FIGURE 15. Results of modelling analysis. The vorticity vector field and the flame front.

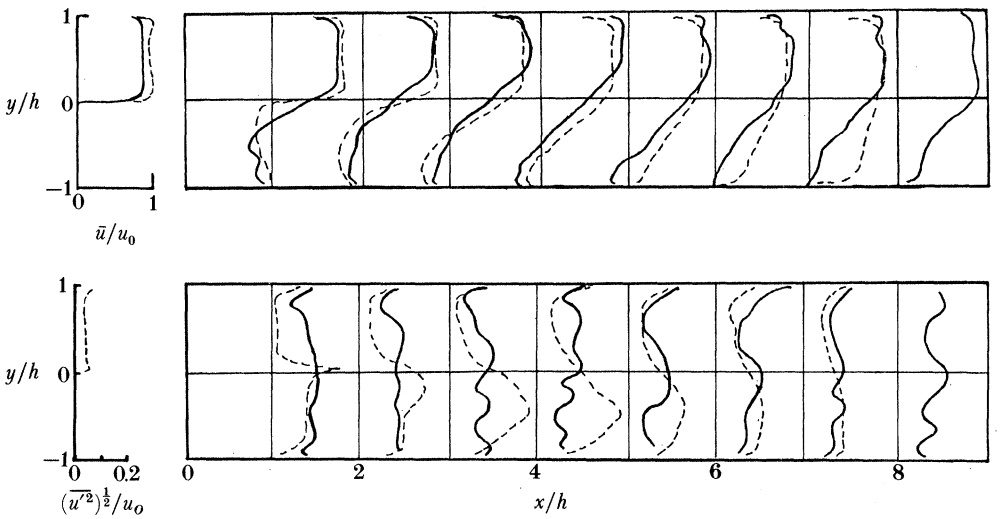

FIGURE 16. Results of modelling analysis. Profiles of the average axial velocity and of the root mean square of its fluctuating component.

keep the burnt medium together as it is eventually swept downstream by the flow of the fresh charge, giving rise to all sorts of large scale flow instabilities (see, for example, Keller *et al.* 1982; Vaneveld *et al.* 1984).

The consequences of these observations bring into focus three rudimentary properties of turbulent flames which hitherto have not been clearly singled out, namely that the mechanism of their motion consists of three components:

(1) advection associated with rotary displacement due to large scale eddies formed in the flow field:

(2) self-advancement, commonly referred to as propagation, associated with chemical transformation from reactants to products taking place at the front;

(3) expansion due to exothermicity whereby each element of mass crossing the flame front undergoes a significant increase in specific volume.

To illustrate how these components contribute towards the flame motion, consider the highly idealized case of a planar flow field of a front of burnt gases moving into an unburnt combustible mixture. Both media are considered to behave as incompressible fluids under the influence of a vortex confined in a slice of the flow field in the form of a channel between two straight, parallel, frictionless sides. Since sufficiently far away from the centre, the vortex, irrespectively of its nature, acquires the velocity distribution of an inviscid case, the effects of viscosity can be neglected and the initial flow field treated as that of a potential vortex.

In such circumstances, the problem is governed by the Poisson equation

$$\nabla^2 \Phi = \delta \cdot u_s, \tag{2.14}$$

where Φ is the velocity potential, the source term having been specified by (2.4) and (2.5). The definition of the flow field is completed by the boundary conditions

$$\nabla \Phi \cdot \boldsymbol{n} = 0 \tag{2.15}$$

at the sides.

Flame propagation is formulated as an initial value problem of a Stefan-like interface. For our illustration, consider three cases.:

(1) the motion of the interface is due entirely to advection exerted by the flow field of the vortex contained in the channel;

(2) in addition, the interface is self-advancing at a prescribed normal speed;

(3) furthermore, the interface is displaced by the action of volumetric line sources whose distribution is delineated by its trajectory, their strength being specified by (2.14).

Solutions are obtained by conformal mapping with use of the Schwarz–Christoffel transformation, according to which, for the channel flow

$$\mathrm{d}\zeta/\mathrm{d}z = \pi\zeta, \tag{2.16}$$

so that the space vector in the transformed plane is

$$\zeta = \exp(\pi z), \tag{2.17}$$

where z is the space vector in the physical plane.

The initial velocity vector field is given by the complex potential of a vortex:

$$w \equiv \Phi + \mathrm{i}\Psi = \mathrm{i}\Gamma \ln z, \tag{2.18}$$

PHILOSOPHICAL TRANSACTIONS OF THE ROYAL SOCIETY A MATHEMATICAL, PHYSICAL & ENGINEERING SCIENCES

where the circulation is normalized so that $\Gamma = \pi^{-1}$. Motion of the interface is determined numerically by the use of the SLIC (Simple Line Interface Calculation) code developed by Noh & Woodward (1976) and improved by Chorin (1980) to enhance the space resolution an implement the Huygens principle of flame self-advancement.

The results derived for a particular case of $S_u = 0.4\,|\nabla\Phi|_{\text{at wall}}$ and $V_f = 3$ after 80 time steps, each $1.785 \times 10^{-3}\, h/|\nabla\Phi|_{\text{at wall}}$, where h is the channel width, are displayed in figures 17 and 18.

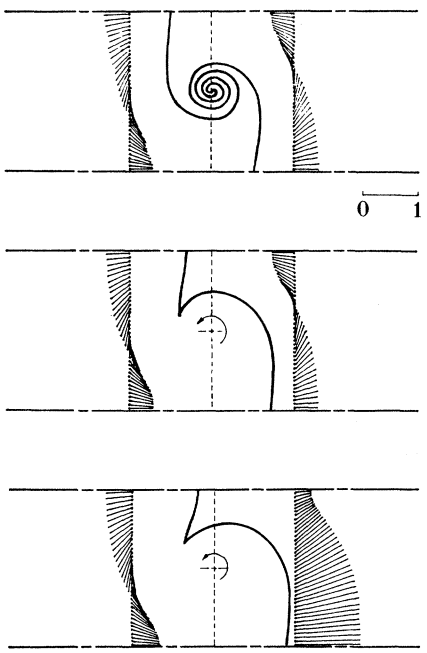

FIGURE 17. Solutions of the elementary components of flame propagation in the physical plane.

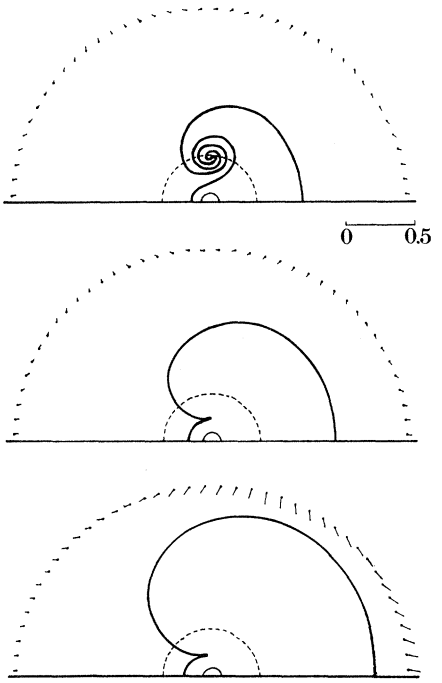

FIGURE 18. Solutions of the elementary components of flame propagation in the transformed plane.

Each figure presents, respectively, solutions for the first, second, and third case specified above; figure 17 in the physical z-plane, and figure 18 in the transformed ζ-plane. Initially the interface was a straight vertical segment denoted by the broken line passing through the vortex centre. The effect of each elementary component of the propagation mechanism is thus expressed by the successive deformation of the front in each of the three consecutive diagrams. Shown on both sides of the deformed front are sets of velocity vectors displayed as straight line segments starting from a row of arbitrarily selected points to which they refer.

The first two cases are entirely passive and therefore exert no influence upon the velocity vector field. However, the third case includes the mechanism of feedback. Surprisingly enough, the only side thereby affected is that of the unburnt mixture, the flow field of the burnt medium remaining completely unchanged. The reason for this is displayed in the transformed plane of figure 18: the domain of the burnt medium is closed within the interface and the side of the channel. The volumetric sources at the front could not, therefore, affect its flow field. The propagation mechanism presented in figure 17 and 18 thus provides a rational reason for most of the salient features of flames described at the outset of this section.

3. Explosion

The exothermicity of combustion manifests itself most distinctly in explosions. The fluid mechanical phenomena associated with them are referred to as blast waves. In its purest form the blast wave is defined as a non-steady, plane-, line-, or point-symmetrical flow field of a compressible medium bounded by a gas-dynamic discontinuity, i.e. a shock or a detonation front.

The literature on blast wave theory is extensive. At first it was inspired by the concern over the effects of nuclear bombs. Thus, during World War II it attracted the attention of many prominent scientists, and fundamental contributions to its development were made by Taylor (1941, 1946), von Neumann (1941), Sedov (1959*a*, *b*), Guderley (1942), Courant & Friedrichs (1948), and their students and associates. Later contributions came from the Russian group of Korobeinikov *et al.* (1961), Grigorian (1958), Chernyi *et al.* (1970), Zeldovich & Raizer (1966), as well as Sakurai (1965), and Jeffrey & Taniuti (1964), to mention just a few.

3.1. *Formulation*

The exposition of the fundamental principles presented here is based primarily on a systematic formalism published over a decade ago (Oppenheim *et al.* 1971) that took into account the effects of non-perfect gas behaviour of the medium, and the influence of sources of mass, momentum, and energy.

According to this formalism, the conservation equations for blast waves can be most conveniently expressed in Eulerian coordinates as follows:

$$\frac{\partial}{\partial t}(\rho r^j a_k) + \frac{\partial}{\partial r}(\rho r^j b_k) = \rho r^j \dot{c}_k. \tag{3.1}$$

Table 2. Matrix of conservation scalars for blast waves

	k	a_k	b_k	$\dot{c}_k$
mass	1	1	1	Ω_1
momentum	2	u	$u+p/\rho u$	$jp/\rho r+\Omega_2$
energy	3	$e+\frac{1}{2}u^2$	$e+\frac{1}{2}u^2+p/\rho$	Ω_3

Here t and r represent the independent variables of time and space respectively and u- the radial velocity at (t, r). The conservation scalars a_k, b_k, and $\dot{c}_k$, are defined in table 2, where p is the pressure, ρ the density, e the specific internal energy, Ω_k $(k = 1, 2, 3)$ the rate of mass supplied from a source, body force, and rate of energy deposited, respectively, all per unit mass of the medium within the blast wave. Also

$$j \equiv \frac{\mathrm{d}\ln A}{\mathrm{d}\ln r} = \begin{cases} 0 \text{ for plane symmetrical flow field,} \\ 1 \text{ for line symmetrical flow field,} \\ 2 \text{ for point symmetrical flow field,} \end{cases}$$

while A is its frontal area.

For the purpose of analysis, the conservation equations (3.1) are transformed by the use of natural blast wave coordinates

$$x = r/r_n \quad \text{and} \quad \tau \equiv t/t_n,$$

where subscript n denotes a point on the trajectory of the front whose motion is described in terms of

$$\xi \equiv r_n/r_0 \quad \text{and} \quad \eta \equiv t_n/t_0.$$

The trajectory is expressed by the use of one of the following parameters:
the front strength, related directly to its Mach number Ma_n

$$y \equiv 1/Ma_n^2;$$

the so-called decay coefficient

$$\lambda \equiv \frac{\mathrm{d}\ln y}{\mathrm{d}\ln \xi};$$

or the front velocity modulus, the slope of its trajectory in the logarithmic time–space plane,

$$\mu \equiv \frac{\mathrm{d}\ln \xi}{\mathrm{d}\ln \eta}.$$

Since the velocity of sound in the atmosphere ahead of the front is usually constant, the two last mentioned are interrelated by the equation

$$\frac{\mathrm{d}\ln \mu}{\mathrm{d}\ln \xi} = \frac{1}{\mu} - \tfrac{1}{2}(\lambda + 2),$$

which follows immediately from their definitions. Also, for the sake of convenience, the dependent variables are normalized by the introduction of the following non-dimensional quantities

$$h \equiv \rho/\rho_n; \quad g \equiv p/\rho_a w_n^2;$$

$$f \equiv u/w_n; \quad \sigma \equiv e/w_n^2 = (\gamma - 1)^{-1} p/\rho w_n^2,$$

where w_n expresses the velocity of the front and subscript a refers to the ambient atmosphere into which it propagates. The last expression is a consequence of the assumption that the medium behaves essentially as a perfect gas with constant specific heats.

Finally – the essential element of the formalism – one introduces the following reduced blast wave coordinates:

$$F \equiv ut/\mu r = f/x \quad \text{and} \quad Z \equiv (at/\mu r)^2 = \Gamma g/hx^2.$$

By virtue of these transformations, the independent variables x and ξ are made to appear only in differential terms, so that the governing equations can be reduced to an autonomous form:

$$\left(\frac{\partial \ln \boldsymbol{A}_l}{\partial \ln x}\right)_\xi = \frac{\boldsymbol{B}_l(F, Z, \boldsymbol{X}_l)}{\boldsymbol{D}(F, Z)}, \tag{3.2}$$

where

$$\boldsymbol{D} \equiv (1-F)^2 - Z,$$

while

$$\boldsymbol{X}_l \equiv \left(\frac{\partial \ln \boldsymbol{A}_l}{\partial \ln \xi}\right)_x = \lambda \left(\frac{\partial \ln \boldsymbol{A}_l}{\partial \ln y}\right)_x.$$

There are four equations in the set of (3.2). Their variables and functions are listed in table 3.

By dividing the first two equations of (3.2) by each other, that is those for $l = 1$ and $l = 2$,

one obtains an expression for the governing equation of the problem in the following concise form:

$$\left[\frac{\partial \ln Z}{\partial \ln (1-F)}\right]_y = \frac{\boldsymbol{P}(F, Z, \boldsymbol{X}_l)}{\boldsymbol{Q}(F, Z, \boldsymbol{X}_l)}. \tag{3.3}$$

The above specifies the phase space for blast waves. Its coordinates are F, Z and y. Seeking a solution to a given problem is tantamount to the determination of an integral curve in this space. The knowledge of singularities is of essential importance; for this reason they are listed in table 4.

TABLE 3. VARIABLES, FUNCTIONS AND PARAMETERS OF BLAST WAVE EQUATIONS IN AUTONOMOUS FORM

l	$\boldsymbol{A}_l$	$\boldsymbol{B}_l$	α_l
1	$1-F$	$\boldsymbol{Q} \equiv F(\alpha_1 - F) + (j+1)\frac{\alpha_3 - F}{1-F} Z$	$\frac{1}{2}(\lambda+2) + (1-\iota)\,\boldsymbol{X}_1$
2	Z	$\boldsymbol{P} \equiv \frac{\Gamma-1}{1-F}\boldsymbol{Q} + [(j+1)(\gamma-1)+2]\frac{\alpha_2 - F}{1-F}\boldsymbol{D}$	$\frac{\lambda+2-\boldsymbol{X}_2}{(j+1)(\Gamma-1)+2}$
3	g	$\boldsymbol{G} \equiv \boldsymbol{Q} + (j+1)(\alpha_3 - F)\,\boldsymbol{D}$	$\frac{\Gamma\lambda - \boldsymbol{X}_3}{(j+1)\Gamma}$
4	h	$\boldsymbol{H} \equiv \boldsymbol{Q} - [(j+1)F - \alpha_4]\,\boldsymbol{D}$	$\boldsymbol{X}_4$

TABLE 4. PHASE SPACE SINGULARITIES

(For definitions of α_l ($l = 1, 2, 3$) see table 3.)

singularity	significance	condition	coordinates F	coordinates Z
A	wave containing a weak discontinuity	$\boldsymbol{P}=0;\ \boldsymbol{Q}=0;\ \boldsymbol{D}=0$	$p-(p^3-q)^{\frac{1}{2}}$†	$(1-F)^2$
B	strong point explosion ($\lambda = j+1,\ y=0$)	$\boldsymbol{P}=0;\ \boldsymbol{Q}=0;\ \boldsymbol{D}\neq 0$	α_2	$\frac{F(\alpha_1-F)(1-F)}{(j+1)(F-\alpha_3)}$
C	wave driven by a cold ($T=0$) piston	$F=1;\ Z=0$	1	0
D	centre of an explosion wave	$\boldsymbol{Q}=\infty;\ Z=\infty$	α_3	∞
E	wave driven by a hot ($T=\infty$) piston	$F=1;\ Z=\infty$	1	∞
F	cold ($T=0$) boundary condition	$\boldsymbol{Q}=0;\ Z=0$	α_1	0
G	strong implosion wave ($y=0$)	$\boldsymbol{P}=0;\ \boldsymbol{Q}=0;\ \boldsymbol{D}=0$	$p+(p^2-q)^{\frac{1}{2}}$†	$(1-F)^2$
H	wave driven by a piston at constant velocity	$F=1;\ \boldsymbol{P}=0$	1	$Z(y)$
I	flow field behind a piston	$F=\infty;\ Z=\infty$	∞	∞
O	cold state at rest	$F=0;\ Z=0$	0	0

† $p \equiv \frac{1}{2}[(1+j^{-1})(1+\alpha_3) - j^{-1}\alpha_1];\quad q \equiv (1+j^{-1})\alpha_3.$

The solution to any specific problem is, of course, subject to boundary conditions, namely the Hugoniot curve expressing the locus of states behind a discontinuity:

$$Z_n = \tfrac{1}{2}(\gamma-1)\,\frac{F_n + [2/(\gamma-1)]\,P_G}{F_n + (1/\gamma)(P_G - 1)}\,(1-F_n)\,F_n, \tag{3.4}$$

where

$$P_G = 1 + (\gamma-1)\,q/a_a^2. \tag{3.5}$$

Here q expresses the specific energy (i.e. energy per unit mass) deposited at the front. The locus of states behind a shock front is given by the Rankine–Hugoniot curve expressed by (3.4) for $P_G = 1$. The strength of the discontinuity is given by the Rayleigh line equation, i.e.

$$y = Z_n/(1-F_n) - \gamma F_n, \tag{3.6}$$

while the density and pressure are given, respectively, by

$$h_n = 1/(1-F_n) \quad \text{and} \quad g_n = (1/\Gamma)\, Z_n h_n. \tag{3.7}$$

The loci of boundary conditions for exothermic fronts, that is fronts associated with a deposition of energy, evaluated on this basis, for $\Gamma = \gamma = 1.4$ are displayed in figure 19.

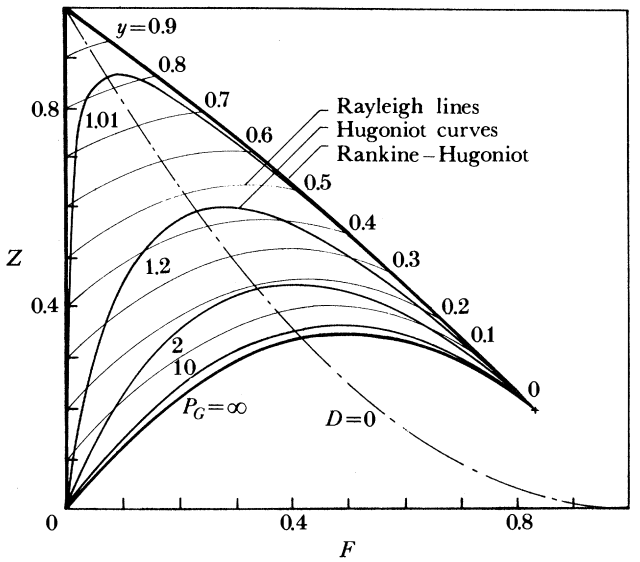

FIGURE 19. Loci of boundary conditions for blast waves (Oppenheim *et al.* 1972).

3.2. *Solutions*

When either $y = 0$ or $\lambda = 0$ all the terms containing y vanish and the problem becomes a function of a single variable, x, while (3.2) become ordinary differential equations; their solutions are then self-similar. An example of such solutions is provided by figure 20, which presents a family of integral curves on the phase plane (F, Z) for self-similar explosions with variable energy deposited at or withdrawn from the front (Barenblatt *et al.* 1980). The $\boldsymbol{D} = 0$ line is the locus of sonic states, that is states where $u = a$, while the $P_n = \infty$ line is the locus of boundary conditions for strong fronts, that is fronts for which $y = 0$. Broken lines are loci of constant x. Each curve corresponds to a fixed value of the flow velocity modulus μ and a corresponding value of the wave-power modulus

$$\epsilon \equiv \mathrm{d}\ln E/\mathrm{d}\ln t = (j+3)\,\mu - 2,\dagger$$

where

$$E \equiv \int_0^{r_n} \left(\frac{1}{\gamma-1}\frac{p}{\rho} + \tfrac{1}{2}u^2\right)\rho r^j\,\mathrm{d}r.$$

Portions of integral curves below the $\boldsymbol{D} = 0$ line correspond to locally supersonic flow.

Of the seven integral curves indicated in figures 20 and 21 the following are of particular interest:

1. blast wave headed by a C.J. detonation front;
2. blast wave headed by a front where energy is deposited at a constant rate;
4. blast wave of constant energy, the classical von Neumann–Taylor–Sedov solution that was

† For derivation of this relation see Barenblatt *et al.* (1980).

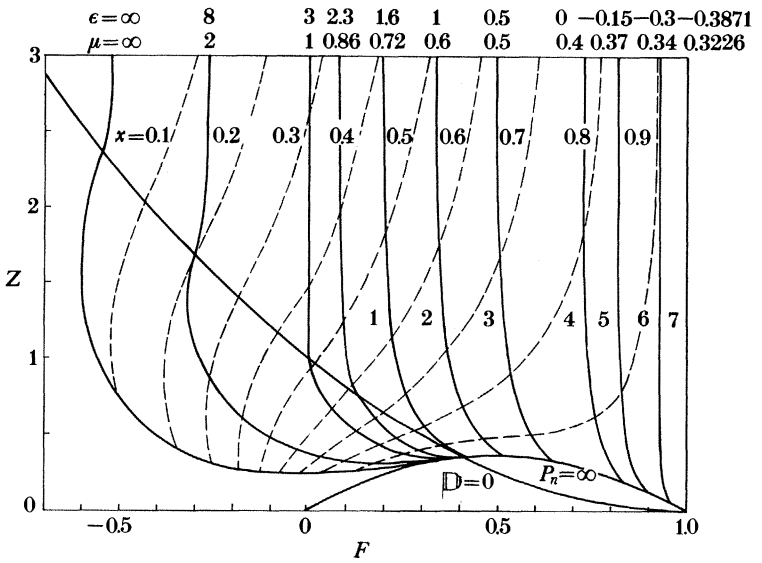

FIGURE 20. Integral curves on the phase plane for self-similar, spherically symmetric blast waves with energy deposition at the front (Barenblatt *et al.* 1980).

obtained to model the atom bomb explosion and predict its yield (a task it accomplished with a remarkable success). Curves to the left of this solution represent exothermic blast waves, waves associated with a deposition of energy at the front; curves to the right of it display endothermic blast waves, waves associated with a withdrawal of energy from the front.

7. The ultimate case of endothermic blast waves corresponding to infinite density ratio at the front.†

Profiles of gas-dynamic parameters for these solutions are depicted in figure 21.

An example of the phase space is provided by figure 22 which presents the solution for the classical case of point explosion generated by the deposition of a finite amount of energy at the centre, propagating into an atmosphere of finite pressure (Kuhl *et al.* 1985). At the plane of $y = 0$ this is the classical von Neumann–Taylor–Sedov solution. As y approaches 1 the blast wave tends to the acoustic limit, its front eventually deteriorating into a sound wave. The corresponding profiles of gas-dynamic parameters are given in figure 23.

The results expressed by continuous lines on figures 22 and 23 have been obtained by approximating the cross-derivatives in terms of a linear interpolation:

$$\boldsymbol{X} = (1-\chi)\left[\frac{\partial \ln \boldsymbol{A}_l}{\partial \ln \xi}\right]_D + \chi\left[\frac{\partial \ln \boldsymbol{A}_l}{\partial \ln \xi}\right]_n, \tag{3.8}$$

where χ is a progress parameter changing from 0 at the centre D to 1 at the front n, while proper approach to the saddle point singularity D (see table 4) at the centre has been carefully assured by matching points between the integral curves. The asymptotic solutions at D are marked on the curves by open dots.

In figure 23 the solutions obtained by Korobeinikov & Sharotova (1969) by using the numerical method of integral relations adopted for this purpose by Korobeinikov & Chushkin (1966) are delineated by broken lines. As can be seen there, these solutions do not behave well near the singularity, an essential difficulty posed by blast wave problems on numerical techniques.

† The cosmological significance of this solution is left to the imagination of the reader.

PHILOSOPHICAL TRANSACTIONS OF THE ROYAL SOCIETY A MATHEMATICAL, PHYSICAL & ENGINEERING SCIENCES

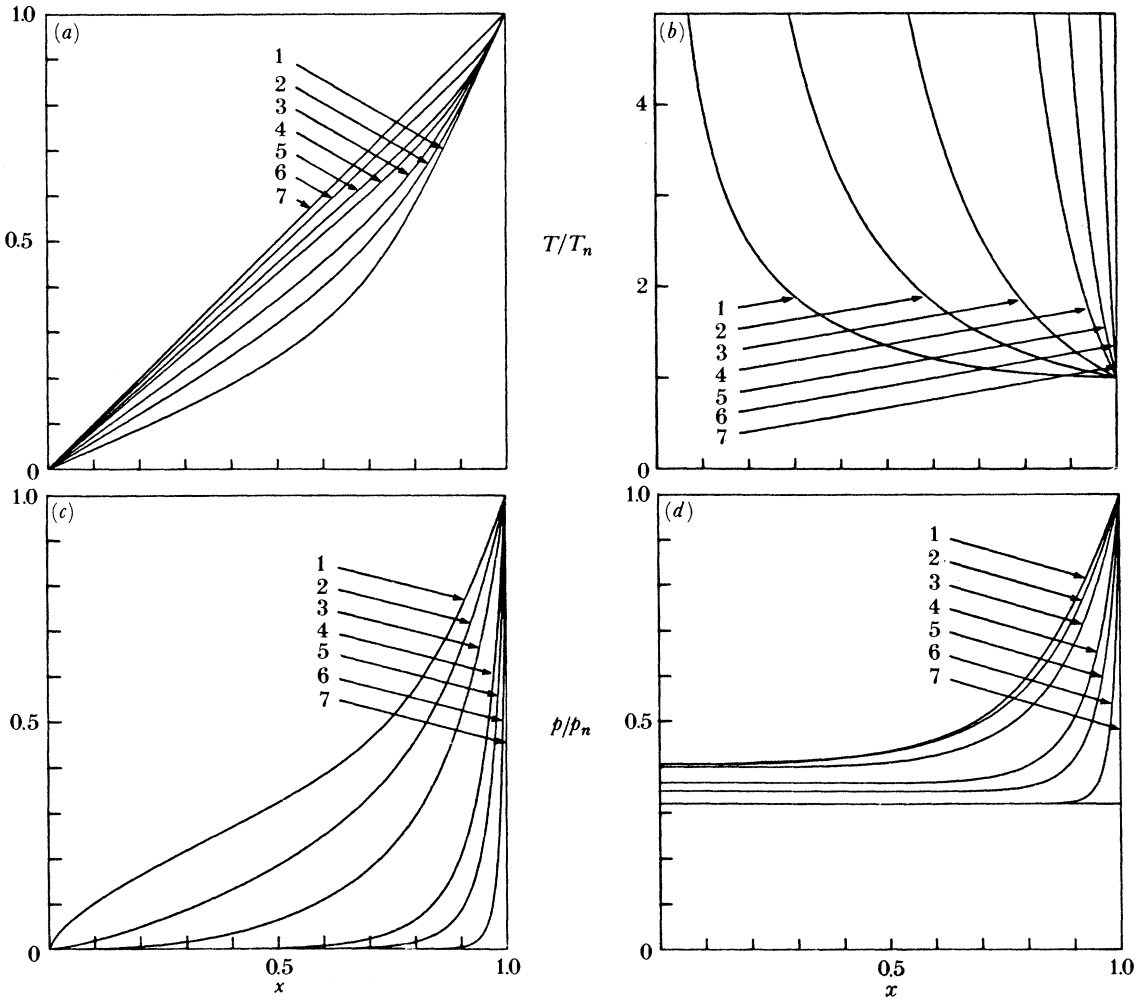

FIGURE 21. Profiles of gas-dynamic parameters of representative cases of figure 20 (Barenblatt *et al.* 1980).

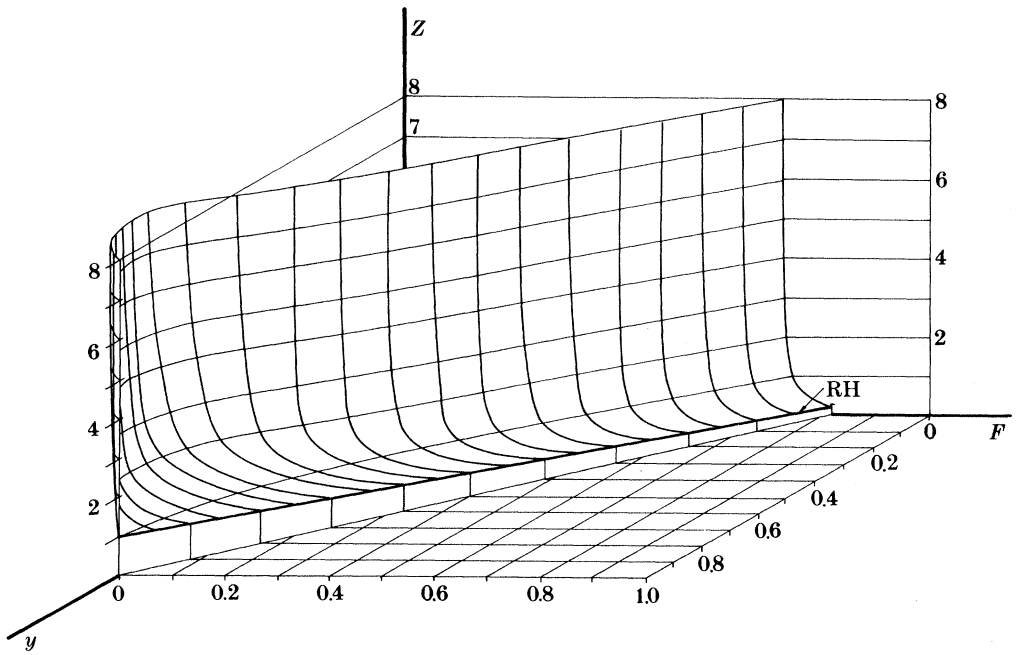

FIGURE 22. Phase space solution for an adiabatic point explosion. (RH denotes the Rankin–Hugoniot line.)

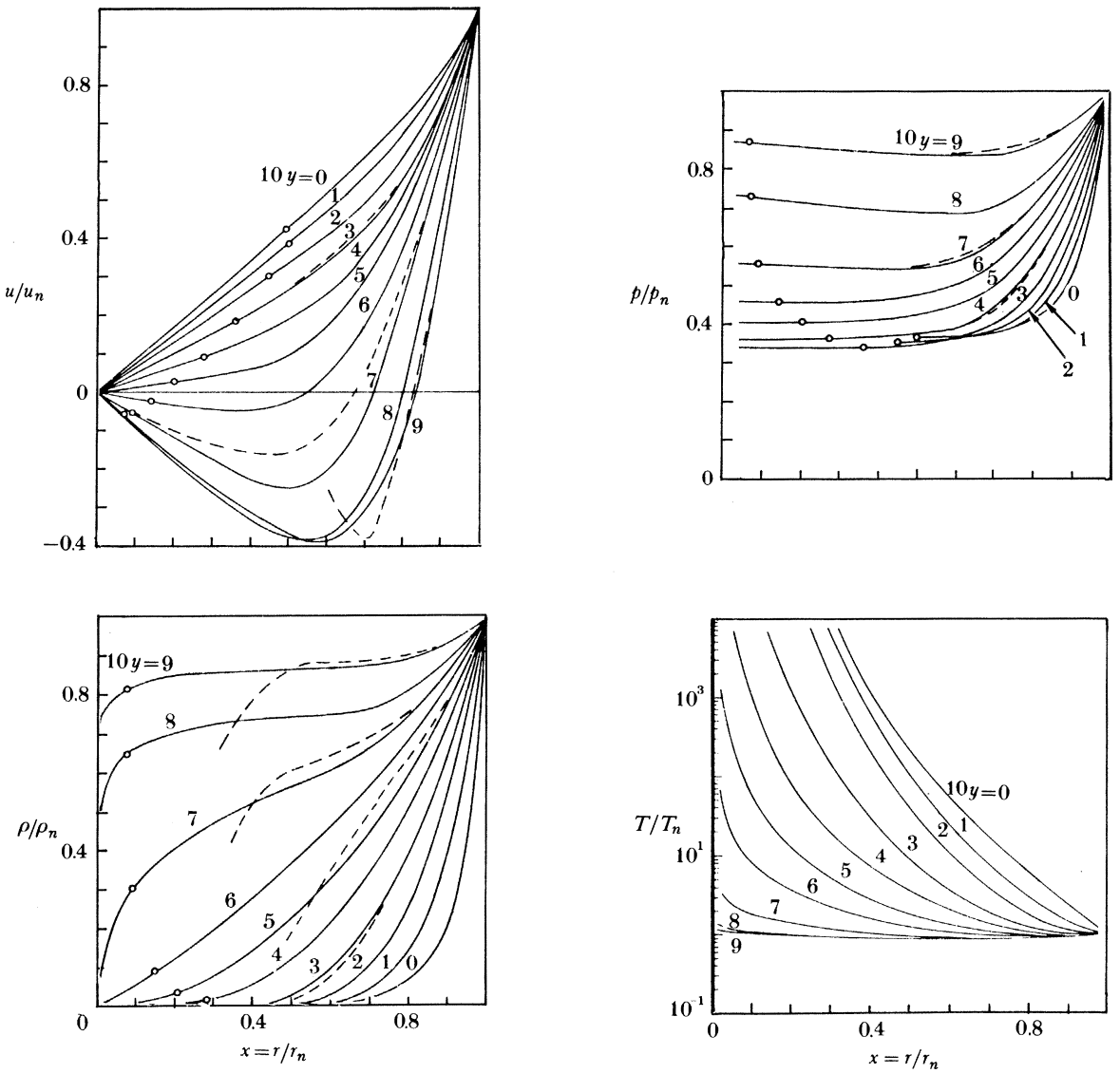

FIGURE 23. Profiles of gas-dynamic parameters for an adiabatic point explosion.

4. DETONATION

All the dynamic effects of combustion treated here are spectacularly displayed in the course of the development of detonation waves and in their structure, a classical subject of research that fascinated combustion scientists from its outset. This was manifested in the papers of Berthelot & Vieille (1822), and Mallard & Le Chatelier (1883), and reflected in the monographs and reviews of Manson (1947), Taylor & Tankin (1958), Zeldovich & Kompaneets (1955), Oppenheim (1961), Soloukhin (1963), Shchelkin & Troshin (1963), Viotsekhovsky *et al.* (1963), Bazhenova *et al.* (1968) and Lee (1977) to mention a few.

4.1. *Development*

Most of the gas-dynamic phenomena associated with the development of detonation in an explosive gas, the process commonly referred to as D.D.T. (Deflagration to Detonation

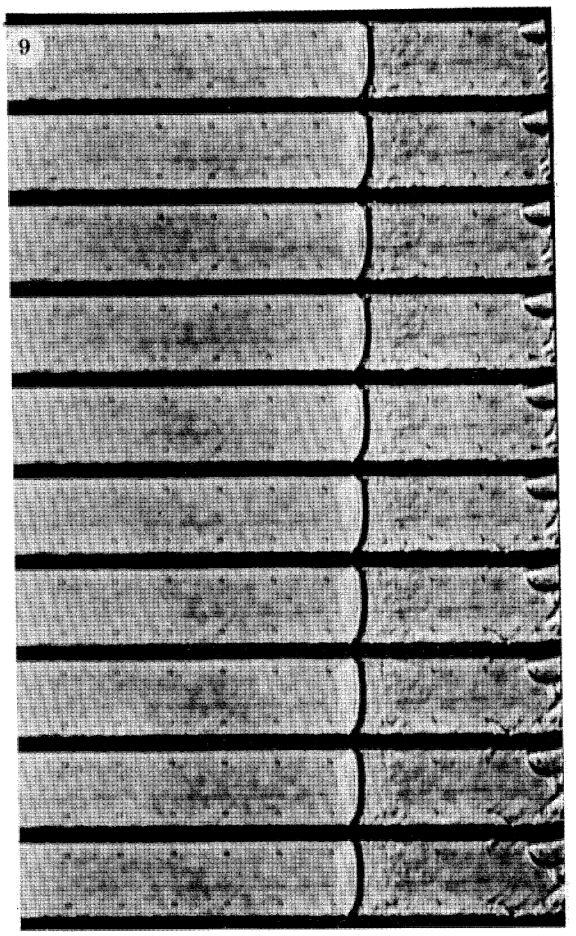

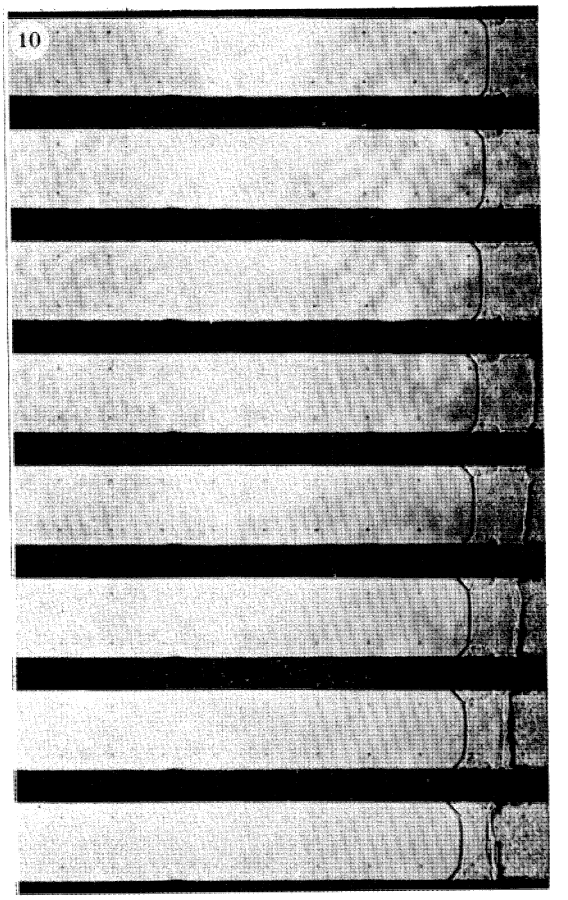

FIGURE 9. Cinematographic schlieren record of mild ignition behind reflected shock front which produces a pressure of 6 atm and a temperature of 1300 K in a stoichiometric iso-octane–oxygen mixture diluted in 70% argon (Vermeer *et al.* 1972). End wall of tube is at right edge of field of view. Sequence is from the top at time intervals of 2 μs between frames.

FIGURE 10. Cinematographic schlieren record of strong ignition obtained under the same conditions as figure 9 but with temperature of 1400 K (Vermeer *et al.* 1972). The photographic conditions are as in figure 9.

PHILOSOPHICAL TRANSACTIONS OF THE ROYAL SOCIETY A MATHEMATICAL, PHYSICAL & ENGINEERING SCIENCES

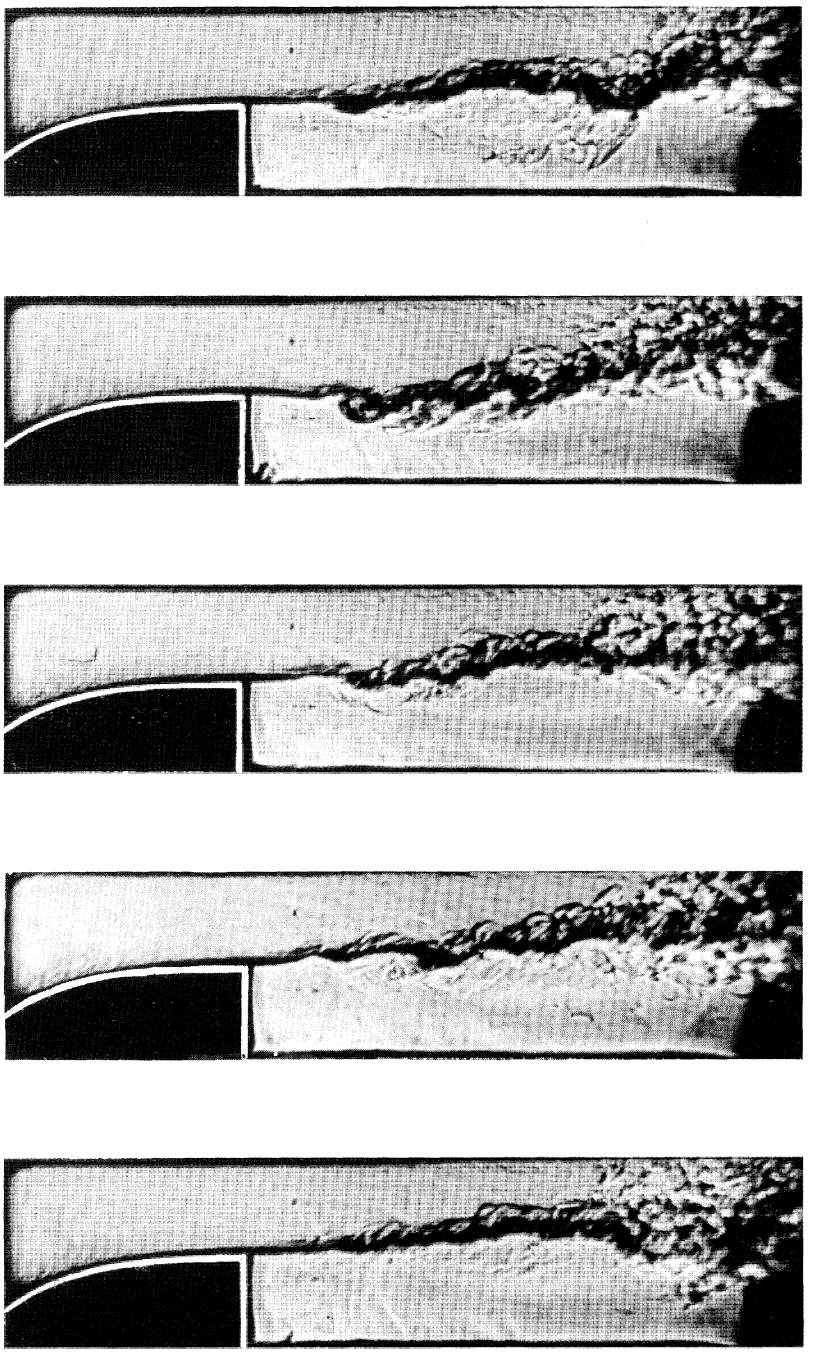

FIGURE 14. Cinematographic schlieren records of turbulent flame in a combustion tunnel. Height of channel is 5 cm. Reynolds number of flow at inlet of 5 cm is around 10^4. Sequence is from the top at intervals of around 19 ms between frames.

PHILOSOPHICAL TRANSACTIONS OF THE ROYAL SOCIETY A MATHEMATICAL, PHYSICAL & ENGINEERING SCIENCES

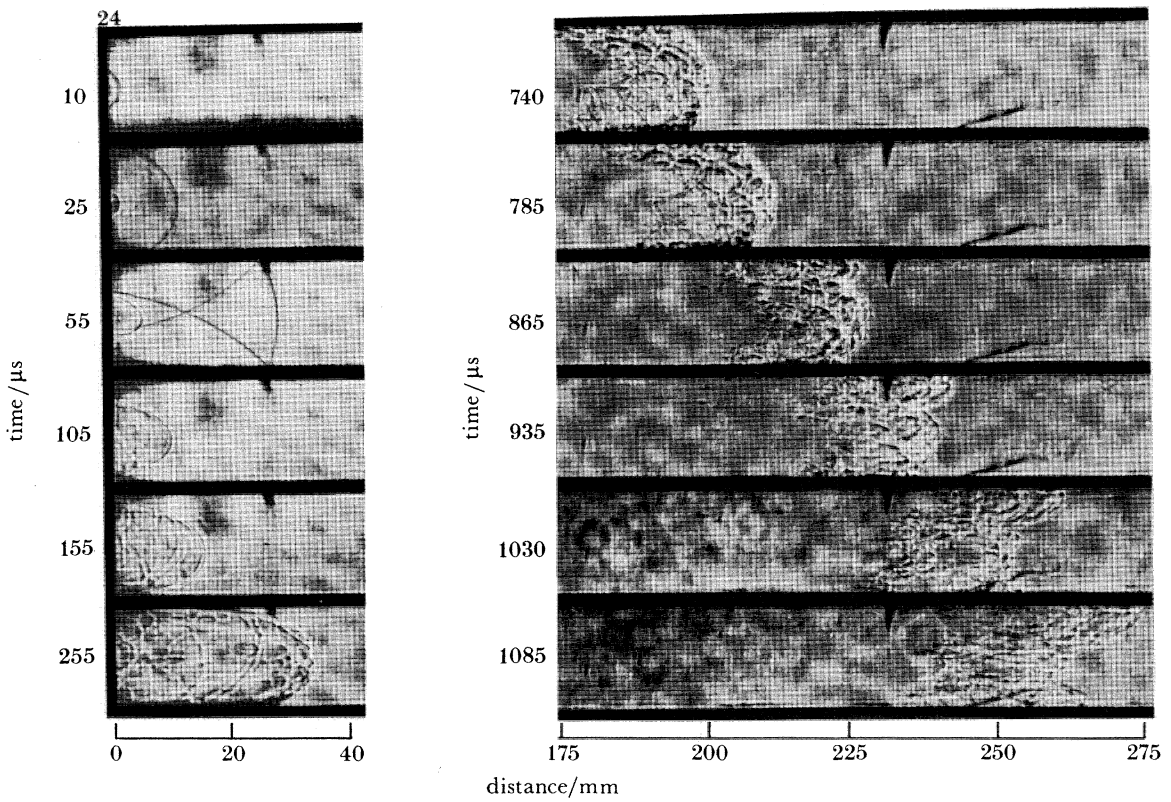

FIGURE 24. Cinematographic schlieren records of ignition, and initial stages of inflammation in a stoichiometric hydrogen–oxygen mixture.

PHILOSOPHICAL TRANSACTIONS OF THE ROYAL SOCIETY A MATHEMATICAL, PHYSICAL & ENGINEERING SCIENCES

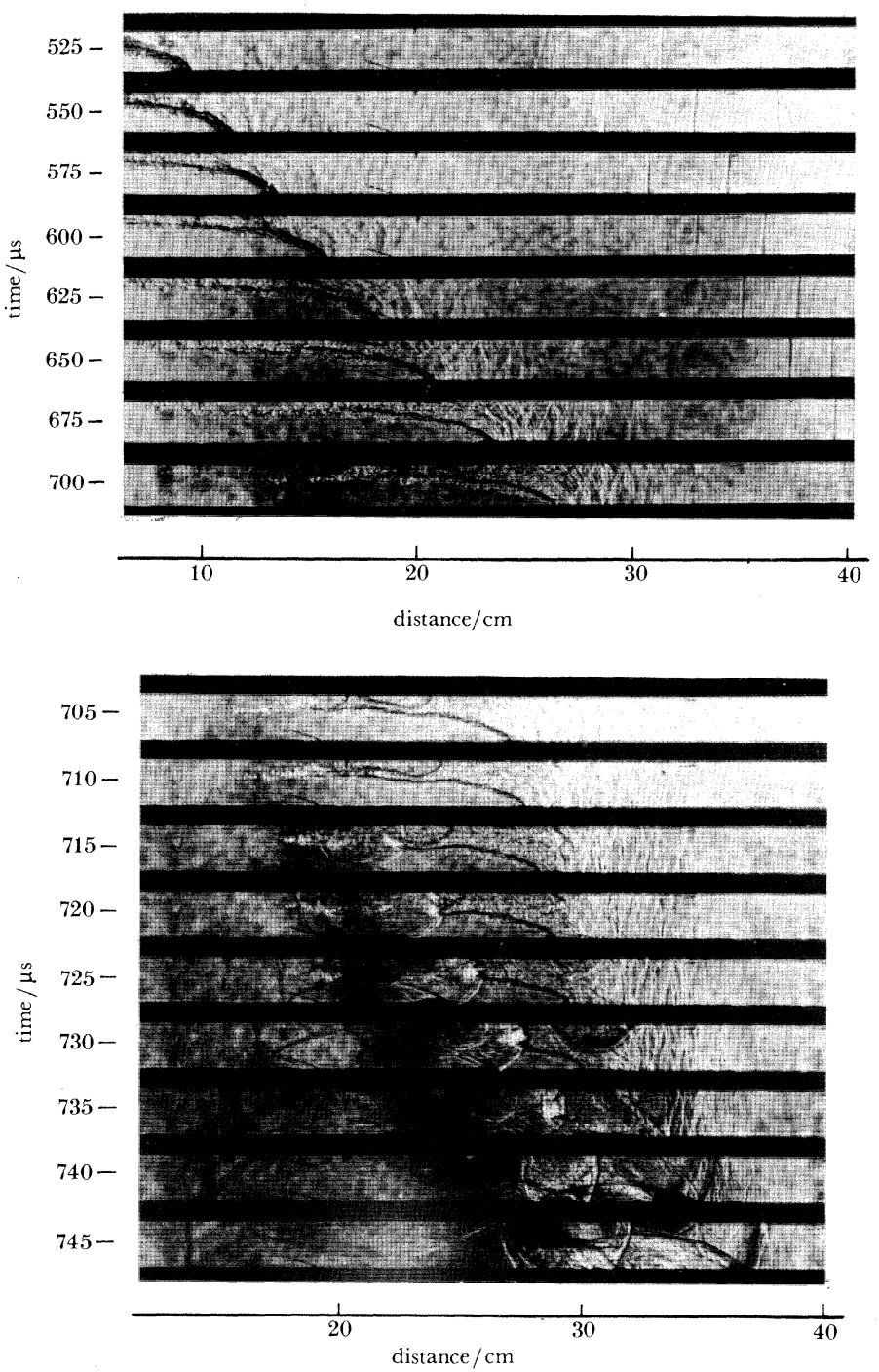

FIGURE 25. Cinematographic schlieren records of intense generation of compression waves by turbulent flame leading to the 'explosion in the explosion' that manifests the transition to detonation (Meyer *et al.* 1970). Later stages of the process depicted in figure 2.

PHILOSOPHICAL TRANSACTIONS OF THE ROYAL SOCIETY A MATHEMATICAL, PHYSICAL & ENGINEERING SCIENCES

PHILOSOPHICAL TRANSACTIONS OF THE ROYAL SOCIETY A MATHEMATICAL, PHYSICAL & ENGINEERING SCIENCES

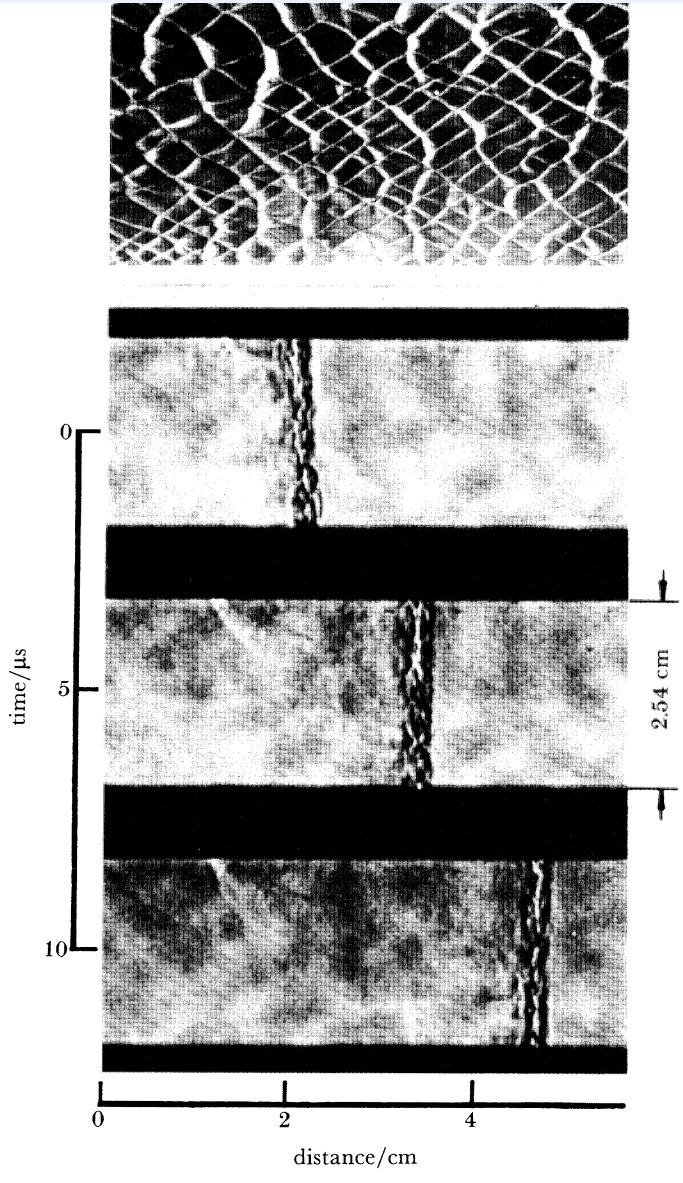

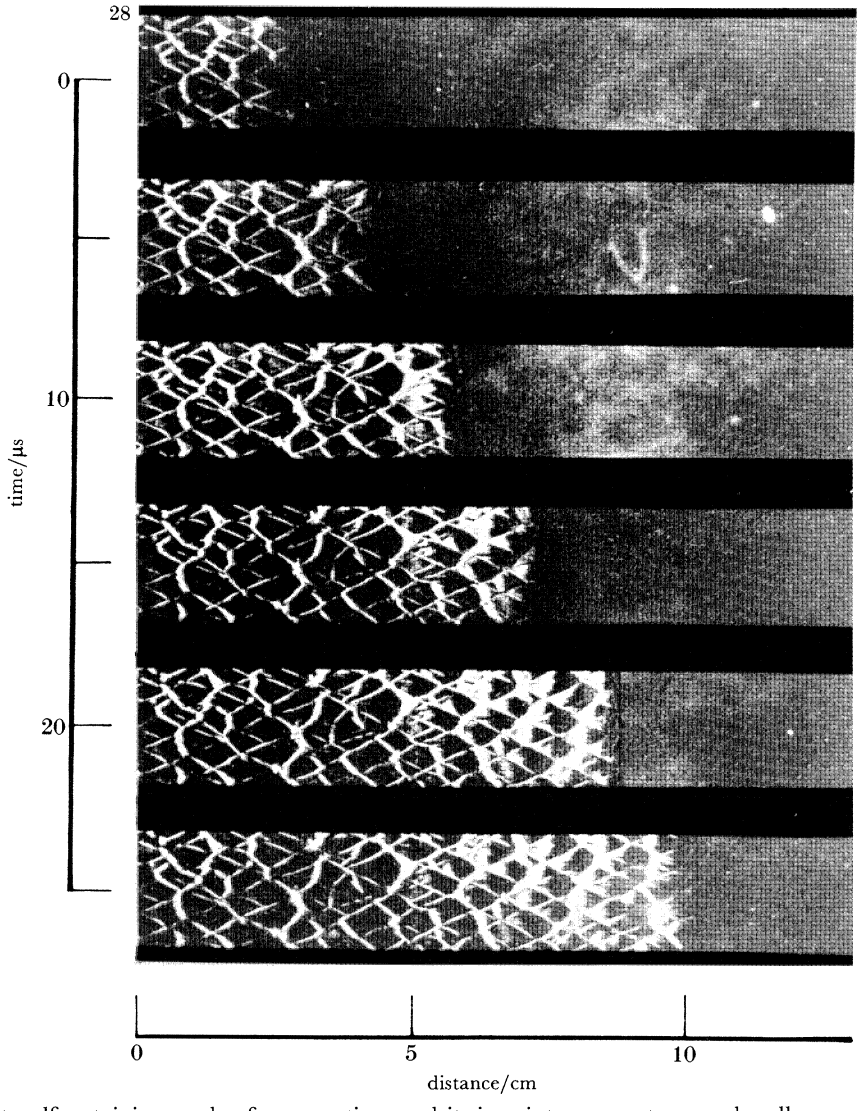

FIGURE 27. Cinematographic schlieren records of a detonation wave in its self-sustaining mode of propagation, and its imprint on a soot covered wall of a rectangular duct, displayed at top. (Oppenheim 1972).

FIGURE 28. Cinematographic schlieren photographs catching the detonation wave in the act of writing on the wall (Oppenheim 1972).

Phil. Trans. R. Soc. Lond. A, *volume* 315 *Oppenheim, plate* 5

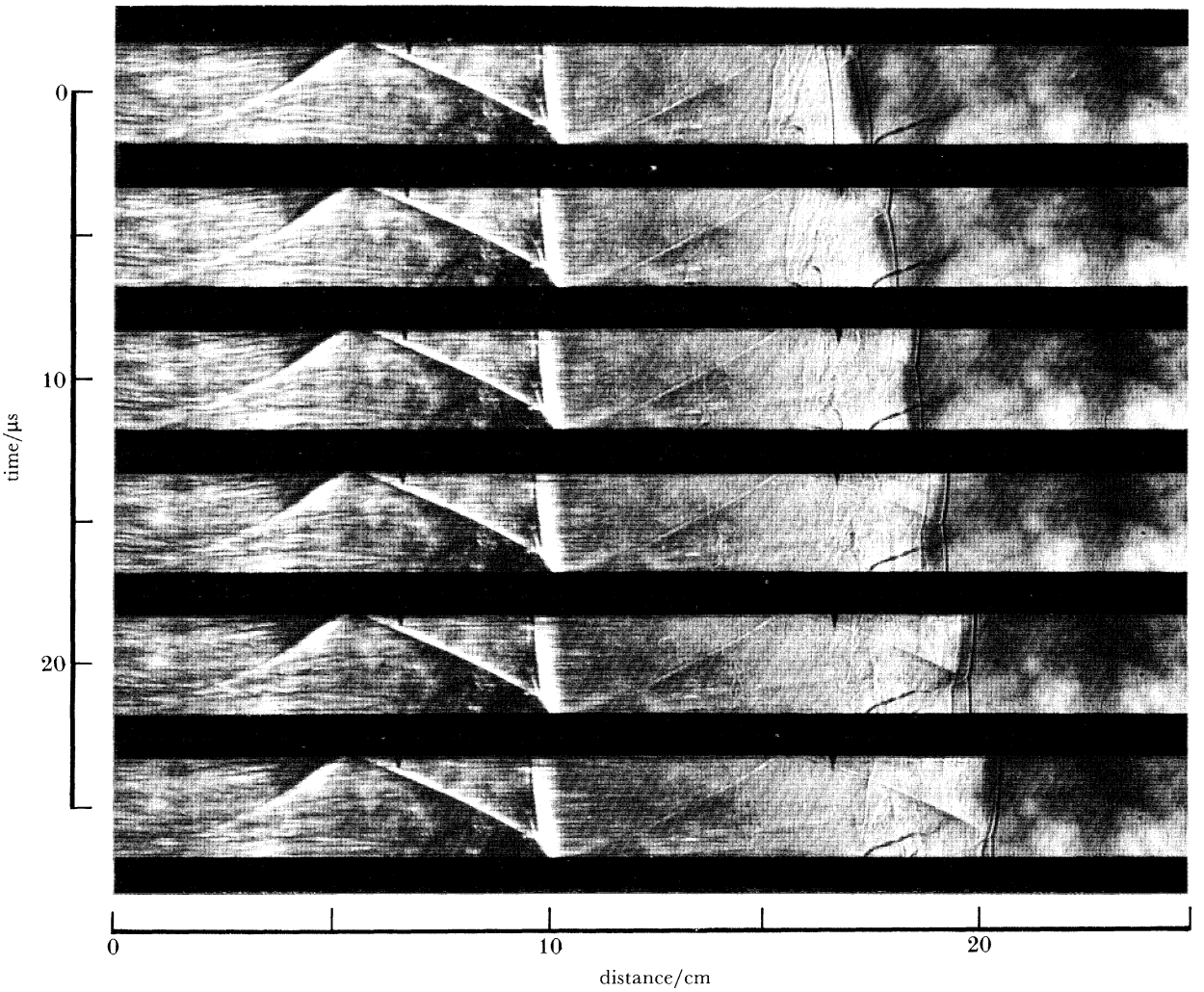

FIGURE 29. A sequence of cinematographic records that reveal the details of the detonation wave front and its action in writing the wall. Structure reduced to a single triple point intersection by proper adjustment of initial conditions (Oppenheim 1972).

PHILOSOPHICAL TRANSACTIONS OF THE ROYAL SOCIETY A MATHEMATICAL, PHYSICAL & ENGINEERING SCIENCES

Transition), have been revealed by high-speed laser schlieren cinematography (Oppenheim & Kamel 1972). Figure 24, plate 3, presents sequences of strips of records, taken at a frequency of 2×10^5 frames per second, of the development of detonation in a stoichiometric hydrogen–oxygen mixture, initially at atmospheric pressure and room temperature, in a 2.54 cm × 3.81 cm cross section tube, ignited by an electric spark at a closed end.

The records show a blast wave formed by the spark followed by a laminar flame of spheroidal shape. The burnt gases act as an accelerating piston formed by the increase in specific volume across the flame front. This causes flame acceleration, associated with the generation of pressure waves ahead of it. These waves coalesce to form shock fronts, of which one is clearly discernible on the last frame in the middle of the figure.

As the flame accelerates further its front acquires a 'tulip' shape, as depicted on the right side of figure 24. This is brought about by rolling eddies at the walls, the Tollmien–Schlichting waves that are formed when the laminar flow structure breaks down, manifesting the onset of a turbulent flame régime. The flame front actually marks the outer boundaries of these rolling eddies.

This leads to a more intense generation of pressure waves, as shown in the upper sequence in figure 25, plate 4, while the shock waves merge ahead of the accelerating flame, causing an increase in the temperature that in turn enhances flame velocity further. This self-augmenting process culminates with an explosion in the exploding medium – a strong ignition (see Urtiew & Oppenheim 1966) – which, as shown in the lower sequence in figure 25, triggers the transition to detonation. There are two such events recorded in this figure, the second producing the detonation wave that emerges on the right side of the cinematographic sequence as a front associated with transverse waves and triple shock intersection, the elementary components of its structure.

Displayed at the top of figure 26 is an enlargement of the frame at 715 μs of figure 24. One can easily discern individual components of the pressure wave ahead of the flame and follow their motion throughout the full cinematographic schlieren record of their propagation. In this way it was possible to construct the time–space diagram of the process presented in figure 26. On this basis we have been able to establish that the pressure wave components we have traced propagate at local sonic velocities, which demonstrates that the pressure wave generated by the accelerating flame just before the onset of detonation is practically isentropic. Thus it was easy to evaluate the state of the gas particle compressed by the pressure wave at the focal point of the 'explosion in the explosion'. We found then (Meyer *et al.* 1970) that the compression alone was not sufficient to produce strong ignition that is necessary for this purpose. It occurs evidently as a consequence of the action of high temperature gases, rich in radicals, that are jetted forth ahead of the accelerating flame by the large scale eddies at the walls, generated in the course of the turbulent flame propagation.

4.2. *Structure*

A cinematographic schlieren record of a self-sustained detonation wave is shown in figure 27, plate 5, together with an imprint it produces on the soot-covered wall of the rectangular duct that contained the explosive mixture. Figure 28, plate 6, presents a cine-sequence of schlieren photographs that caught the detonation wave in the act of writing its imprint on the wall. One of the glass walls of the tube was, for this purpose, coated with a thin layer of soot. This is shown even more clearly in figure 29, where, with the same experimental technique, the initial conditions of the mixture were adjusted by dilution, combined with a sufficiently low initial

PHILOSOPHICAL TRANSACTIONS OF THE ROYAL SOCIETY A MATHEMATICAL, PHYSICAL & ENGINEERING SCIENCES

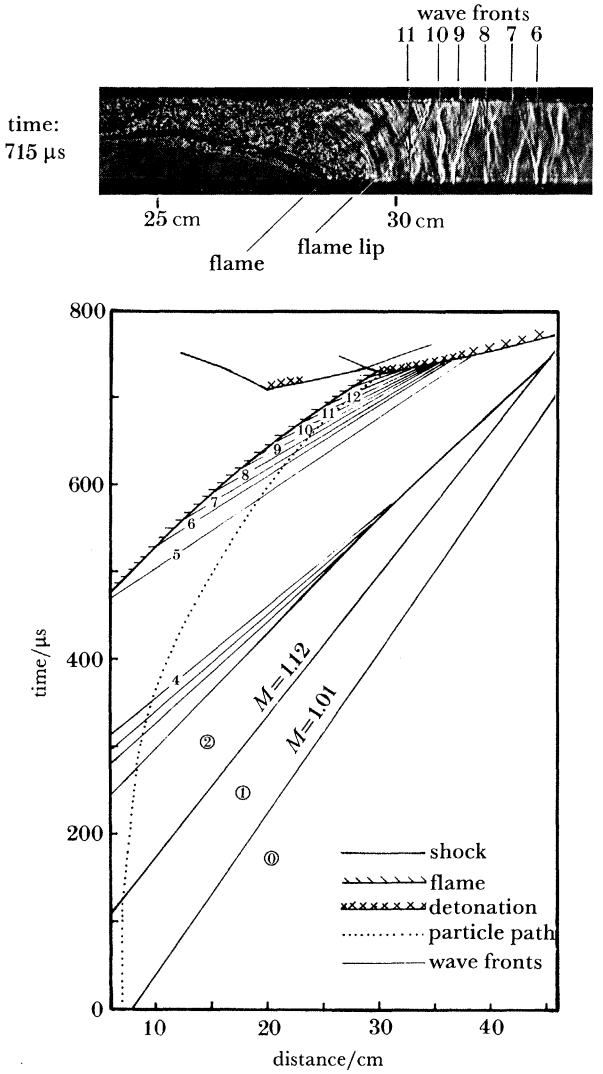

FIGURE 26. Time–space history of gas-dynamic processes associated with the development of detonation depicted in figure 25 (Meyer *et al.* 1970).

pressure, to reduce the number of the 'wall writing heads' to one. The nature of these 'heads' is thereby revealed and the elementary component of the propagation mechanism is elucidated as a collision between the triple wave intersection points, described in figure 30. A schematic diagram of a self-sustained detonation wave, displaying the action of triple wave intersections is given in figure 31. The cellular trajectories are evidently recorded on the wall by the highly concentrated vortices created by shear at contact discontinuities immediately behind points of intersection.

The discovery of the cellular structure of detonation waves was one of the most exciting scientific events of the 1960s. It has been a truly international achievement that combines the pioneering contributions of many investigators. Included prominently among them were Denisov & Troshin (1959), Shchelkin & Troshin (1963) and Soloukhin (1963) in the Soviet Union; Van Tiggelen (1969) in Belgium; Edwards *et al.* (1970) in the U.K.; Lee (1972, 1977) in Canada; Fujiwara (1970, 1975) and Taki & Fujiwara (1981) in Japan; White (1961),

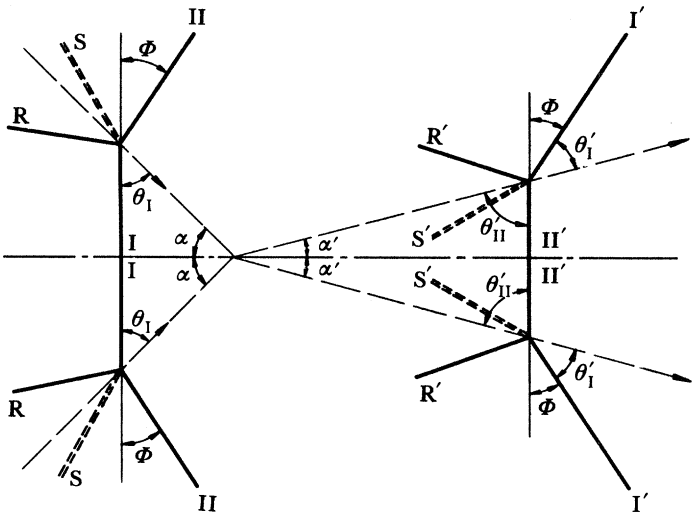

FIGURE 30. Schematic diagram of a collision between triple wave intersections. I: incident shock; II: Mach stem; R: reflected shock; S: slip line.

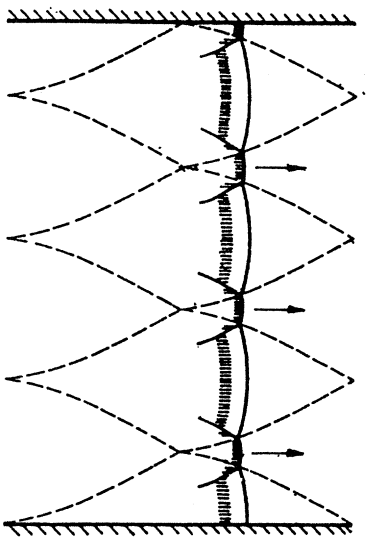

FIGURE 31. Schematic diagram of a self-sustained detonation wave that displays the triple wave intersections and their cellular trajectories.

Strehlow (1968), as recounted by Oppenheim (1965, 1972), Oppenheim *et al.* (1968, 1969) and Oran *et al.* (1981) in the United States.

One of the most interesting features revealed thereby is the exact role played by exothermic centres in the propagation mechanism. Each collision of triple wave intersections creates a state of sufficiently high temperature and pressure to initiate strong ignition. Thereupon, the deflagration tends to lag behind the shock front in its progress along the cellular structure (see figure 31) so that, as pointed out by Lundstrom & Oppenheim (1969), the sustenance of the detonation process depends crucially on the next collision. Hence, for the detonation wave to remain self-sustained, the distance between collisions reflected by the cell size must be properly spaced, which results in its regular structure.

As is evident from this description of the development and structure of detonation, all the topics presented here – ignition, inflammation, and explosion – are of central importance, providing in a single sequence of events a most spectacular illustration of all the dynamic features of combustion brought forth in this paper.

Conclusion

In conclusion I wish to express hope that the comprehensive exposition of the dynamic features of combustion presented here will excite the reader's imagination. It is my expectation that on the recognition that these features represent the primary consequences of the exothermicity of combustion, without which this process would have been of no practical interest, this paper will provide an incentive for future studies. So far, it seems to me, in spite of their profound practical significance, these aspects have been treated somewhat superficially in combustion science.

Since the dynamic effects of exothermicity constitute the major feedback mechanism of the combustion reaction on the flow field where it takes place, acquiring further knowledge in this subject should be instrumental for the development of controlled combustion systems: engines where the explosivity of the process is harnessed to such an extent that the energy provided by the fuel is converted into useful work at maximum efficiency, minimum pollutant emissions, and optimum tolerance to a wide variety of fuels.

The author wishes to express his profound appreciation to his mentor, Sir Owen Saunders, F.R.S., and his friend, Professor F. J. Weinberg, F.R.S., for all the encouragement and criticism they offered in the course of his work on this paper. This work was supported by the Office of Energy Research, Office of Basic Energy Sciences, Division of Engineering, Mathematics, and Geosciences, U.S. Department of Energy under Contract DE-AC03-76SF00098, the National Science Foundation under Grant CPE-8302232, and the NASA Lewis Research Center under Grants NAG 3-131 and NAG 3-137.

References

Barenblatt, G. I., Guirguis, R. H., Kamel, M. M., Khul, A. L., Oppenheim, A. K. & Zeldovich, Ya. B. 1980 Self-similar explosion waves of variable energy at the front. *J. Fluid Mech.* **99**, 841–858.

Baulch, D. L., Drysdale, D. D., Horne, D. G. & Lloyd, A. C. 1972 *Evaluated kinetic data for high temperature reactions*, vol. 1. London: Butterworths.

Bazhenova, T. V., Gvozdeva, L. G., Nobastov, Yu. S., Naboko, I. M., Nemkov, R. G. & Predvoditeleva, O. A. 1968 *Shock waves in real gases*. Moscow: Izdatel'stvo Nauka.

Berthelot, M. & Vieille, P. 1822 Sur la vitesse de propagation des phenomenes explosifs dans les gaz. *C. r. hebd. Séanc. Acad. Sci. Paris* **94**, 101–108; 822–823; **95**, 151–157.

Boddington, T., Gray, P. & Harvey, D. I. 1971 Thermal theory of spontaneous ignition: criticality in bodies of arbitrary shape. *Phil. Trans. R. Soc. Lond.* A **270**, 467–506.

Borisov, A. A. 1974 On the origin of exothermic centers in gaseous mixtures. *Acta astronaut.* **1**, 909–920.

Carter, C. D., Sawyer, R. F. & Oppenheim, A. K. 1985 Thermochemistry of ignition applied to the H_2–O_2 system. (In preparation.)

Chernyi, G. G., Korobeinikov, V. P., Levin, V. A. & Medvedev, S. A. 1970 One-dimensional unsteady motion of combustible gas mixtures associated with detonation waves. *Acta astronaut.* **15**, 255–266.

Chorin, A. J. 1973 Numerical studies of slightly viscous flow. *J. Fluid Mech.* **57**, 785–796.

Chorin, A. J. 1978 Vortex sheet approximation of boundary layers. *J. comp. Phys.* **27**, 428–442.

Chorin, A. J. 1980 Flame advection and propagation algorithms. *J. comp. Phys.* **35**, 1–11.

Clarke, J. F., Kassoy, D. R. & Riley, N. 1984 Shocks generated in a continued gas due to rapid heat addition at the boundary; I. Weak shock waves and II. Strong shock waves. *Proc. R. Soc. Lond.* A **393**, 309–329; 331–351.

PHILOSOPHICAL TRANSACTIONS OF THE ROYAL SOCIETY A MATHEMATICAL, PHYSICAL & ENGINEERING SCIENCES

Cohen, L. M. & Oppenheim, A. K. 1975 Effects of size and dilution on dynamic properties of exothermic centers. *Combust. Flame* **25**, 207–211.

Cohen, L. M., Short, J. M. & Oppenheim, A. K. 1975*c* A computational technique for the evaluation of dynamic effects of exothermic reactions. *Combust. Flame* **24**, 319–334.

Courant, R. & Friedrichs, K. O. 1948 *Supersonic flow and shock waves*. New York: Wiley.

Denisov, Yu. N. & Troshin, Ya. K. 1959 Pulsiruyushchaia i spinovaia detonatsia gazovikh smeshei v trubakh (Pulsating and spinning detonation of gaseous mixtures in tubes). *Dokl. Akad. Nauk SSSR* **125**, 110–113.

Dixon-Lewis, G. 1979 Kinetic mechanism, structure and properties of premixed flames in hydrogen–oxygen–nitrogen mixtures. *Phil. Trans. R. Soc. Lond.* A **292**, 45–99.

Dougherty, E. P. & Rabitz, H. 1980 Computational kinetics and sensitivity analysis of hydrogen–oxygen combustion. *J. chem. Phys.* **72**, 6571–6585.

Edwards, D. H., Hooper, G., Job, E. M. & Parry, D. J. 1970 The behavior of the frontal and transverse shocks in gaseous detonation waves. *Astronaut. Acta* **15**, 323–333.

Frank-Kamenetskii, D. A. 1969 *Diffusion and heat transfer in chemical kinetics* (transl. N. Thon). New York: Plenum Press. (Revised edition of text published in 1947.)

Fujiwara, T. 1970 Plane steady Navier–Stokes detonations of oxyozone. *J. Phys. Soc. Japan* **29**, 1350–1364.

Fujiwara, T. 1975 Spherical ignition of oxyhydrogen behind a reflected shock wave. In *Fifteenth Symposium (International) on Combustion*, pp. 1515–1524. Pittsburgh: The Combustion Institute.

Gear, C. W. 1971 *Numerical initial value problems in ordinary differential equations*. New Jersey: Prentice-Hall.

Ghoniem, A. F., Chorin, A. J. & Oppenheim, A. K. 1982 Numerical modelling of turbulent flow in a combustion tunnel. *Phil Trans. R. Soc. Lond.* A **394**, 303–325.

Gray, P. & Lee, P. R. 1967 Thermal explosion theory. *Oxidation and Combustion Reviews* **2**, pp. 1–183. Amsterdam: Elsevier.

Gray, B. F. & Yang, C. H. 1965 On the unification of the thermal and chain theories of explosion limits. *J. phys. Chem.* **69**, 2747–2750.

Grigorian, S. S. 1958 Cauchy's problem and the problem of a piston for one-dimensional nonsteady motions of a gas. *J. appl. Math. Mech.* **22**, 187–197.

Guderley, G. 1942 Powerful spherical and cylindrical compression shocks in the neighbourhood of a centre of a sphere and of a cylinder axis. *Luftfarhrtforschung* **19**, 302–312.

Guirguis, R. H., Oppenheim, A. K., Karasalo, I. & Creighton, J. R. 1981 Thermochemistry of methane ignition. *Prog. Astronaut. Aeronaut.* **76**, 134–153.

Hicks, B. L. 1954 Theory of ignition considered as a thermal reaction. *J. chem. Phys.* **22**, 414–429.

Hsiao, C.-C., Ghoniem, A. F., Chorin, A. J. & Oppenheim, A. K. 1985 Numerical simulation of a turbulent flame stabilized behind a rearward-facing step. In *Proceedings of the twentieth (international) symposium on combustion*. Pittsburgh: The Combustion Institute. (In the press.)

Jeffrey, A. & Taniuti, T. 1964 *Nonlinear wave propagation with applications to physics and magnetohydrodynamics*. New York: Academic Press.

Kassoy, D. R. & Poland, J. 1980 The thermal explosion confined by a constant temperature boundary: I—The induction period solution. *J. appl. Math.* **39**, 412–430.

Kassoy, D. R. & Poland, J. 1981 The thermal explosion confined by a constant temperature boundary. II—The extremely rapid transient. *J. appl. Math.* **41**, 231–246.

Keller, J. O., Vaneveld, L., Korschelt, D., Hubbard, G. L., Ghoniem, A. F., Daily, J. W. & Oppenheim, A. K. 1982 Mechanism of instabilities in turbulent combustion leading flashback. *AIAAerospace Jl* **20**, 254–262.

Kindelan, M. & Williams, F. A. 1975 Radiant ignition of a combustible solid with gas phase exothermicity. *Acta astronaut.* **2**, 955–980.

Korobeinikov, V. P. & Chushkin, P. I. 1966 Plane cylindrical, and spherical explosions in a gas with counter pressure. *Proc. V. A. Steklov Inst. Math.* (ed. L. I. Sedov), pp. 4–33. Moscow: Izdatel'stvo Nauka.

Korobeinikov, V. P., Mil'nikova, N. S. & Ryazanov, Ye. V. 1961 *The theory of point explosion*. Moscow: Fizmatgiz; (transl. by U.S. Department of Commerce, JPRS: 14, 334, CSO: 6961-N, Washington, D.C. (1962)).

Korobeinikov, V. P. & Sharotova, K. V. 1969 *Gasdynamic functions of point explosions*. Moscow: Computer Center, USSR Academy of Sciences.

Kuhl, A. L., Kamel, M. M. & Oppenheim, A. K. 1985 Application of the principle of self-similarity to the analysis of non-self-similar blast waves. (In preparation.)

Lee, J. H. S. 1972 Gasdynamics of detonation. *Astronaut. Acta* **17**, 455–466.

Lee, J. H. S. 1977 Initiation of gaseous detonation. *Ann. Rev. phys. Chem.* **28**, 75–104.

Levin, V. A. & Chernyi, G. G. 1967 Asymptotic laws of behaviour of detonation waves. *J. appl. Math. Mech.* **31**, 393–405.

Lewis, B. & von Elbe, G. 1961 *Combustion flames and explosions of gases*. (xix + 731 pages.) New York: Academic Press. (Revised edition of text published in 1951.)

Libouton, J. C., Dormal, M. & Van Tiggelen, P. J. 1981 Reinitiation process at the end of the detonation cell. Gasdynamics of detonations and explosions. *Prog. Astronaut. Aeronaut.* **75**, 358–369.

Liñan, A. & Williams, F. A. 1970 Theory of ignition of a reactive solid by constant energy flux. *Comb. Sci. Technol.* **2**, 11–20.

PHILOSOPHICAL TRANSACTIONS OF THE ROYAL SOCIETY A MATHEMATICAL, PHYSICAL & ENGINEERING SCIENCES

Lundstrom, E. A. & Oppenheim, A. K. 1969 On the influence of non-steadiness on the thickness of the detonation wave. *Proc. R. Soc. Lond.* A **310**, 463–478.

Mallard, E. & Le Chatelier, H. 1883 Recherches experimentales et theoriques sur la combustion des melanges gaseux explosifs. *Ann. Mines* **8**, 274–568.

Manson, N. 1947 *Propagation des detonations et des deflagrations dans les melanges gazeaux*. Paris: ONERA and l'Institut Francais des Petroles. (Transl. as ASTIA AD. no. 132-808).

Merzhanov, A. G. & Averson, A. E. 1971 The present state of the thermal ignition theory: an invited review *Combust. Flame* **16**, 89–124.

Meyer, J. W. & Oppenheim, A. K. 1971*a* On the shock-induced ignition of explosive gases. In *Thirteenth Symposium (International) on Combustion*, pp. 1153–1164. Pittsburgh: The Combustion Institute.

Meyer, J. W. & Oppenheim, A. K. 1971*b* Coherence theory of the strong ignition limit. *Combust. Flame* **17**, 65–68.

Meyer, J. W., Urtiew, P. A. & Oppenheim, A. K. 1970 On the inadequacy of gasdynamic processes for triggering the transition to detonation. *Combust. Flame* **14**, 13–20.

von Neumann, J. 1941 The point source solution. First published in *N.D.R.C., Div. B., Rep.* no. AM-9. 1944 In *Shock hydrodynamics and blast waves* (ed. H. A. Bethe). AECD-2860. 1947 Revised version in *Blast waves* (ed. H. A. Bethe). Los Alamos Scientific Laboratory Rep. no. LA-2000, 27–55. 1963 Reprinted in *John von Neumann collected works* (ed. A. H. Taub), vol. 6, pp. 219–237. New York: Pergamon Press.

von Neumann, J. & Goldstine, H. 195 Blast wave calculation. *Communs pure appl. Math.* **8**, 327–353. (Reprinted in *John von Neumann collected works* (ed. A. H. Taub), vol VI, pp. 386–412. New York: Pergamon Press.)

Noh, W. T. & Woodward, P. 1976 SLIC (Simple Line Interface Calculation). In *Proc. 5th Int. Conf. Num. Math. Fluid Mech.*, pp. 330–339. Berlin: Springer-Verlag.

Oppenheim, A. K. 1961 Development and structure of plane detonation waves. *Fourth AGARD Combustion and Propulsion Colloquium, Milan, Italy, April* 1960, pp. 186–258. London: Pergamon Press.

Oppenheim, A. K. 1965 Novel insight into the structure and development of detonation. *Acta astronaut.* **11**, 6, 391–400.

Oppenheim, A. K. 1972 *Introduction to gasdynamics of explosions*. Courses and Lectures no. 48 of The International Centre for Mechanical Science, Udine. (V+220 pages.) New York: Springer-Verlag.

Oppenheim, A. K. 1982 Dynamic effects of combustion. In *Proceedings of the Ninth U.S. National Congress of Applied Mechanics*, pp. 29–40. New York: The American Society of Mechanical Engineers.

Oppenheim, A. K., Cohen, L. M., Short, J. M., Cheng, R. K. & Hom, K. 1975*a* Dynamics of the exothermic process in combustion. In *Fifteenth Symposium (International) on Combustion*, pp. 1503–1513. Pittsburgh: The Combustion Institute.

Oppenheim, A. K., Cohen, L. M., Short, J. M., Cheng, R. K. & Hom, K. 1975*b* Shock tube studies of exothermic processes in combustion. *Modern Developments in Shock Tube Research*, pp. 557–574. *Proceedings of the Tenth International Shock Tube Symposium*. Japan: Kyoto University.

Oppenheim, A. K. & Ghoniem, A. F. 1983 Aerodynamic features of turbulent flames. *AIAAerospace Paper* no. 83-0470, 10 pp.

Oppenheim, A. K. & Kamel, M. M. 1972 *Laser cinematography of explosions*. Courses and Lectures no. 100 of The International Centre for Mechanical Sciences, Udine. (226 pages.) New York: Springer-Verlag.

Oppenheim, A. K., Kuhl, A. L., Lundstrom, E. A. & Kamel, M. M. 1972 A parametric study of self-similar blast waves. *J. Fluid Mech.* **52**, 657–682.

Oppenheim, A. K., Lee, J. H. & Soloukhin, R. I. 1969 Current views on gaseous detonation. *Acta astronaut.* **14**, 5, 565–584.

Oppenheim, A. K., Lundstrom, E. A., Kuhl, A. L. & Kamel, M. M. 1971 A systematic exposition of the conservation equations for blast waves. *J. appl. Mech.* **38**, 783–794.

Oran, E. S., Bonis, J. P., Young, T., Flanigan, M., Barks, T. & Picone, M. 1981 Numerical simulation of detonations in hydrogen–air and methane–air mixtures. *Eighteenth Symposium (International) on Combustion*, pp. 1641–1649. Pittsburgh: The Combustion Institute.

Poland, J., Hindash, I. O. & Kassoy, D. R. 1982 Ignition processes in confined thermal explosions. *Combustion Science and Technology* **27**, 215–227.

Sakurai, A. 1965 Blast wave theory. *Basic developments in fluid dynamics*, vol. 1 (ed. M. Holt), pp. 309–375. New York: Academic Press.

Saytzev, S. G. & Soloukhin, R. I. 1962 Study of combustion of an adiabatically-heated mixture. In *Eighth Symposium (International) on Combustion*, pp. 344–347. Baltimore: The Williams and Wilkins Co.

Sedov, L. I. 1959*a* Propagation of strong explosion waves. *Prikl. Mat. Mekh.* **10**, 241–250.

Sedov, L. I. 1959*b* One dimensional unsteady motion of a gas. In *Similarity and dimensional method in mechanics* (transl. by M. Friedman, ed. by M. Holt), ch. IV, pp. 146–295. Fourth Printing, New York: Academic Press.

Semenov, N. N. 1935 *Chemical kinetics and reactions*. Oxford: Clarendon Press.

Semenov, N. N. 1943 On types of kinetic curves in chain reactions. I. Laws of the autocatalytic type. *Dokl. Akad. Nauk SSSR* XLII, **8**, 342–348.

Semenov, N. N. 1944*a* On types of kinetic curves in chain reactions. II. Consideration of the interaction of active particles. *Dokl. Akad. Nauk SSSR* XLIV, **2**, 62–66.

PHILOSOPHICAL TRANSACTIONS OF THE ROYAL SOCIETY A MATHEMATICAL, PHYSICAL & ENGINEERING SCIENCES

Semenov, N. N. 1944*b* On types of kinetic curves in chain reactions. Allowance for chain rupture on walls of reaction vessel in the case of oxidation of hydrogen. *Dokl. Akad. Nauk SSSR* XLIV, **6**, 241–245.
Semenov, N. N. 1958 *Some problems in chemical kinetics and reactivity* (transl. by M. Boudart), volume 1. (xii + 239 pages.) Princeton University Press.
Semenov, N. N. 1959 *Some problems in chemical kinetics and reactivity* (transl. by M. Boudart), volume 2. (ix + 331 pages.) Princeton University Press.
Shchelkin, K. I. & Troshin, Ya. K. 1963 *Gazodinamika goreniya*. Moscow: Izdatel'stvo Akademii Nauk SSSR. (Transl. by B. W. Kuvshinoff 1966. Baltimore: Mono Book Corp.)
Sokolik, A. S. 1960 *Self-ignition flame and detonation in gases*. Moscow: Izdatel'stvo Akademii Nauk SSSR. (Transl. by N. Kaner 1963. Jerusalem: Israel Program for Scientific Translations.) Available from Washington: U.S. Department of Commerce, Office of Technical Services, OTS 63-11179; NASA TT F-125.
Soloukhin, R. I. 1963 *Udarnye volny i detonatsia v gazakh*. Moscow: Gosudarstvennoye Izdatel'stvo Fiziko-matematycheskoi Literatury. (Transl. by B. W. Kuvshinoff 1966. Baltimore: Mono Book Corp.)
Strehlow, R. A. 1968 Gas phase detonations: recent developments. *Combust. Flame* **12**, 2, 81–101.
Taki, S. & Fujiwara, T. 1981 Numerical simulation of triple shock behavior of gaseous detonation. In *Eighteenth Symposium (International) on Combustion*, pp. 1671–1681. Pittsburgh: The Combustion Institute.
Taylor, G. I. 1941 The formation of a blast wave by a very intense explosion. British Report RC-210. 1950, revised version in *Proc. R. Soc. Lond.* A **201**, 175–186.
Taylor, G. I. 1946 The air wave surrounding an expanding sphere. *Proc. R. Soc. Lond.* A **186**, 273–292.
Taylor, G. I. & Tankin, R. S. 1958 Gas dynamical aspects of detonation. In *Gasdynamics of combustion and detonation*, (ed. H. W. Emmons) ch. 3, pp. 622–686. Princeton: Princeton University Press.
Urtiew, P. E. & Oppenheim, A. K. 1966 Experimental observations of the transition to detonation in an explosive gas. *Proc. R. Soc. Lond.* A **295**, 13–28.
Van Tiggelen, P. J. 1969 On the minimal initial size of an explosive reaction center. *Combust. Sci. Technol.* **1**, 225–232.
Van't Hoff, J. H. 1896 *Studies in chemical dynamics*. London: Williams & Norgate.
Vaneveld, L., Hom, K. & Oppenheim, A. K. 1984 Secondary effects in combustion instabilities leading to flashback. *AIAAerospace Jl* **22**, 81–82.
Vermeer, D. J., Meyer, J. W. & Oppenheim, A. K. 1972 Auto-ignition of hydrocarbons behind reflected shock waves. *Combust. Flame* **18**, 327–336.
Voitsekhovsky, B. V., Mitrofanov, V. V. & Topchian, M. E. 1963 *Struktura fronta detonatsii v gazakh* (Structure of the detonation front in gases.) Novosibirsk: Izd. Sib. Otd. ANSSSR (Transl. by B. W. Kuvshinov & L. Holtschlag 1965. Baltimore: Mono Book Corp.)
Voyevodsky, V. V. & Soloukhin, R. I. 1965 On the mechanism and explosion limits of hydrogen–oxygen chain self-ignition in shock waves. In *Tenth Symposium (International) on Combustion*, pp. 279–283. Pittsburgh: The Combustion Institute.
Warnatz, J. 1984 Survey of rate coefficients in the C/H/O system. In *Chemistry of combustion* (ed. W. C. Gardiner, Jr, ch. 5, pp. 197–360. Wien, New York: Springer-Verlag.
White, D. R. 1961 Turbulent structure of gaseous detonation. *Phys. Fluids* **4**, 465–480.
Yang, C. H. & Gray, B. F. 1967 The determination of explosion limits from a unified thermal chain theory. In *Eleventh symposium (international) on combustion*, pp. 1099–1106. Pittsburgh: The Combustion Institute.
Zajac, L. J. & Oppenheim, A. K. 1971 Dynamics of an explosive reaction center. *AIAAerospace Jl* **9**, 545–553.
Zeldovich, Ya. B. & Kompaneets, A. S. 1955 *Teoriya detonatsii*. Moscow: Gostekhizdat. (Transl. as *Theory of detonation*. New York: Academic Press (1960)).
Zeldovich, Ya. B. & Raizer, Yu. P. 1966 *Physics of shock waves and high temperature hydrodynamic phenomena* (2nd edn). Moscow: Izdatel'stvo Nauka. (Transl. by W. D. Hayes, ed. by R. F. Probstein. New York: Academic Press (1967)).
Zeldovich, Ya. B., Barenblatt, G. I., Librovich, V. B. & Machviladze, G. M. 1980 *Mathematical theory of combustion and explosion* (478 *pages*.) Moscow: Izdatel'stvo Nauka.

Appendix. Notation

symbol

A	pre-exponential coefficient in (1.2)
$\boldsymbol{A}$	generalized dependent variable in (3.2) specified in table 3
a	velocity of sound, or conservation scalar in (3.1) and table 2
$\boldsymbol{B}$	generalized dependent variable in (3.2) specified in table 3
b	conservation scalar in (3.1) and table 2

c specific heat of a chemical species in (3.1) and table 2
$\hat{c}$ specific heat of a gas mixture
$\tilde{c}$ specific heat per unit mole
$\boldsymbol{D}$ generalized variable in (3.1), $(1-F)^2-Z$
E activation energy, or blast wave energy
e specific internal energy
F pressure function, $P^{(r-1)/r}-1$, or reduced blast wave coordinate
f normalized velocity, u/w_{n}
g normalized pressure, $p/\rho_0 w_{\mathrm{n}}^2$
H overall heat transfer coefficient
h specific enthalpy, or channel width, or density ratio, ρ/ρ_0
$\tilde{h}$ specific enthalpy per unit mole
I total number of chemical species in a reacting mixture
J total number of chemical reactions
j index reflecting the geometry of a blast wave, $\mathrm{d}\ln A/\mathrm{d}\ln r_{\mathrm{n}}$
k reaction rate constant
$\dot{\boldsymbol{L}}$ loss rate in (1.15)
l volume to area ratio
M_i molecular mass
Ma Mach number
N number density of exothermic kernels
$\boldsymbol{n}$ normal unit vector
P pressure ratio
$\boldsymbol{P}$ function of reduced blast wave coordinates and cross-derivatives specified in table 3
$\dot{\boldsymbol{P}}$ compression rate in (1.15)
p pressure
Q normalized exothermic energy
$\dot{Q}$ normalized exothermic power
$\boldsymbol{Q}$ function of reduced blast wave coordinates and cross-derivatives specified in table 3
$\dot{\boldsymbol{Q}}$ exothermicity rate in (1.15)
q specific exothermic energy, or heat transfer
R normalized radius at the kernel,
Re Reynolds number
$\mathscr{R}$ universal gas constant
r reaction rate, or radius
S normal burning speed
$\boldsymbol{s}$ tangential unit vector
T temperature
t time
U normalized velocity,
u velocity scalar, or axial velocity component
$\boldsymbol{u}$ velocity vector
V specific volume ratio
v specific volume
W volumetric expansion rate, $\mathrm{d}\ln V/\mathrm{d}\eta$

w front velocity
X chemical species
(X) concentration expressed in the number of moles per unit mass
$\boldsymbol{X}$ generalized cross-derivative in (3.2) specified in table 3
x normalized space coordinate, r/r_n
Y mass fraction
y front strength, Ma_n^{-2}
$\boldsymbol{Z}$ vector of chemical species constituting a mixture, or reduced blast-wave coordinate
Z number of moles per unit mass in a gas mixture, $\Sigma_{i=1}^{I}(X_i)$
z space vector in the physical plane
β Hugoniot asymptote, $(\Gamma-1)/(\Gamma+1)$
Γ isentropic exponent, $-(\partial \ln \rho/\partial \ln v)_\phi$
γ specific heat ratio, c_p/c_v
δ effective duration of exothermic power-pulse, or Kronecker delta function
ϵ blast wave power modulus, $\mathrm{d} \ln E/\mathrm{d} \ln t$
ζ space vector of the transformed plane
η normalized time, $a_0 t/r_0$, or normalized time coordinate of the front, t_n/t_0
Θ normalized temperature of the kernel, T_k/T_0
θ normalized time, t/δ
κ index reflecting the geometry of the kernel, $(j+1)^{-1}$
λ front decay coefficient, $\mathrm{d} \ln y/\mathrm{d} \ln \xi$
μ front velocity modulus, $\mathrm{d} \ln \bar{\xi}/\mathrm{d} \ln y$
ν stoichiometric coefficient
ξ vorticity, or normalized front coordinate
ρ density
σ standard deviation in temperature, or normalized internal energy, e/w_n^2
τ time period, or normalized time coordinate
Φ velocity potential
λ progress parameter in (3.7)
Ψ Hugoniot parameter, or stream function
ω standard deviation in induction-time complex velocity potential

subscripts

a ambient conditions
b burnt medium
D point singularity at the centre of a blast wave
e internal energy
f forward direction, or flame
G point on the Hugoniot curve corresponding to initial specific volume
h enthalpy
i given chemical species, or induction period
j given chemical reaction
k kernel, or index of conservation principles in (3.1) and table 2
l either f or r, or index in (3.2) and table 3
m mean

n point on the trajectory of the front
o initial condition, or a fixed point on the trajectory of the front
p constant pressure
r reverse direction
s surroundings
t thermal period
u unburnt medium
ν constant specific volume
ϵ divergence component of velocity
ζ solenoidal component of velocity
ϕ constant entropy

PHILOSOPHICAL TRANSACTIONS OF THE ROYAL SOCIETY A MATHEMATICAL, PHYSICAL & ENGINEERING SCIENCES

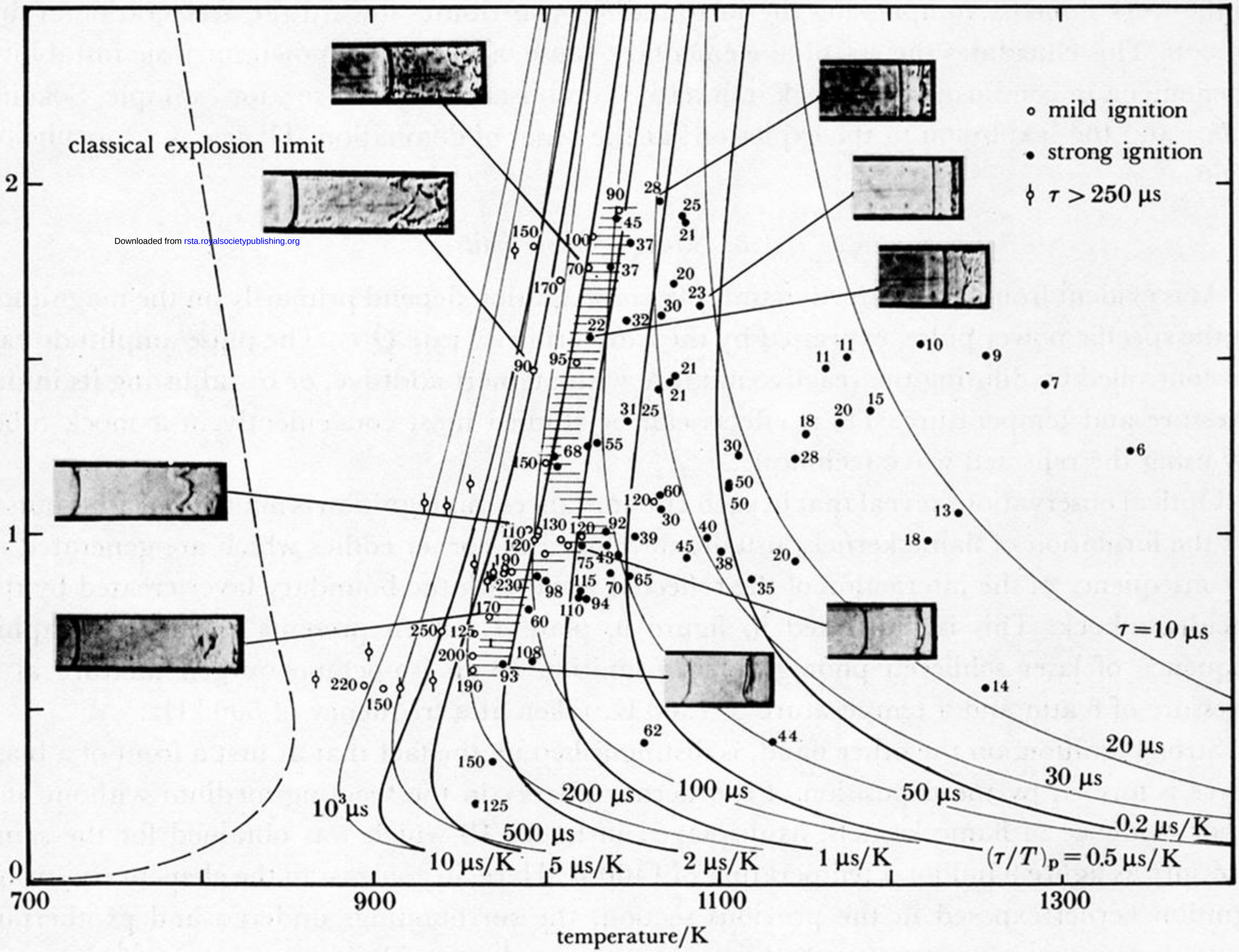

FIGURE 11. Strong ignition limit – the demarcation between mild and strong ignitions – for the stoichiometric hydrogen–oxygen system (Meyer & Oppenheim 1971*a*).

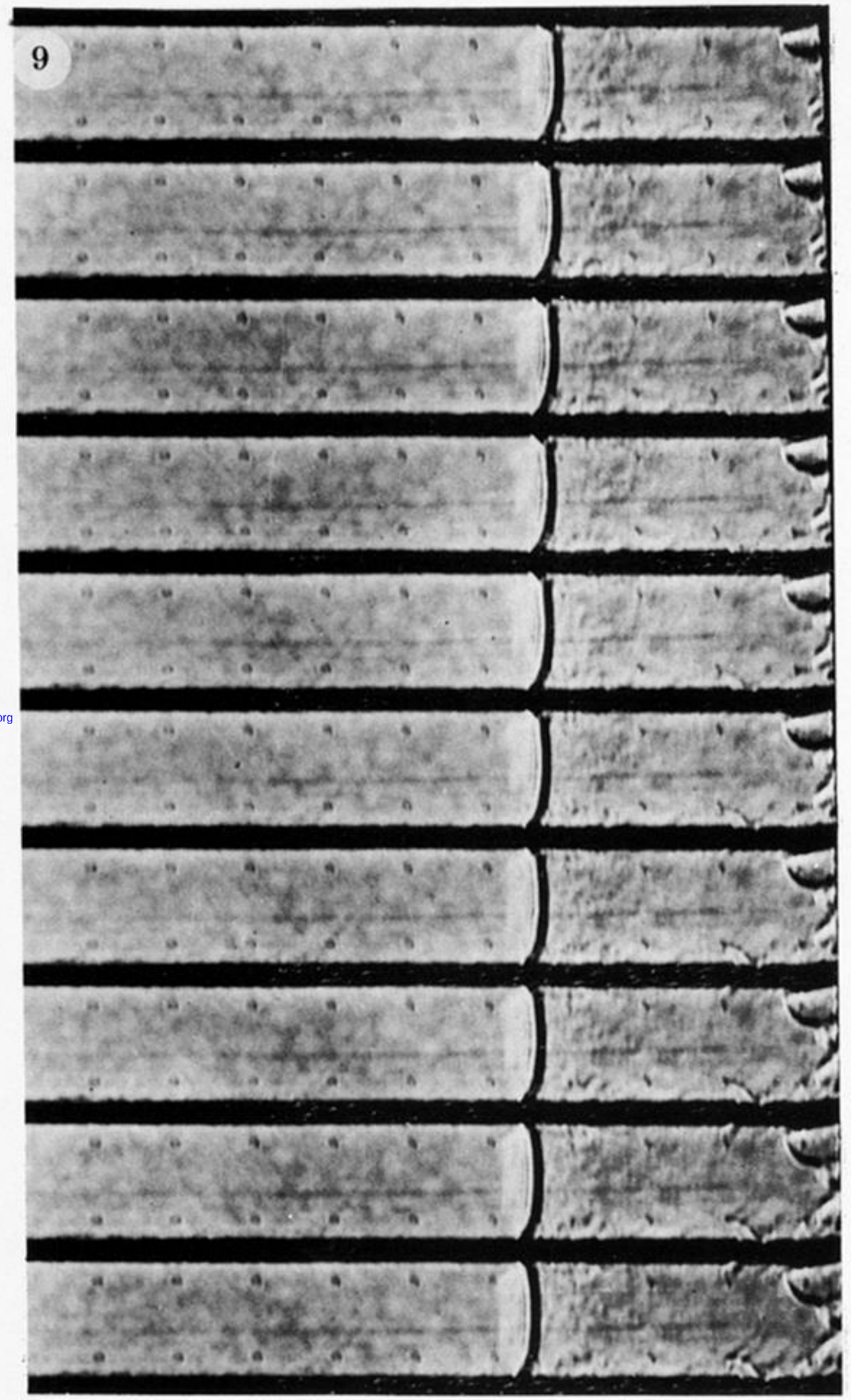

FIGURE 9. Cinematographic schlieren record of mild ignition behind reflected shock front which produces a pressure of 6 atm and a temperature of 1300 K in a stoichiometric iso-octane–oxygen mixture diluted in 70% argon (Vermeer *et al.* 1972). End wall of tube is at right edge of field of view. Sequence is from the top at time intervals of 2 μs between frames.

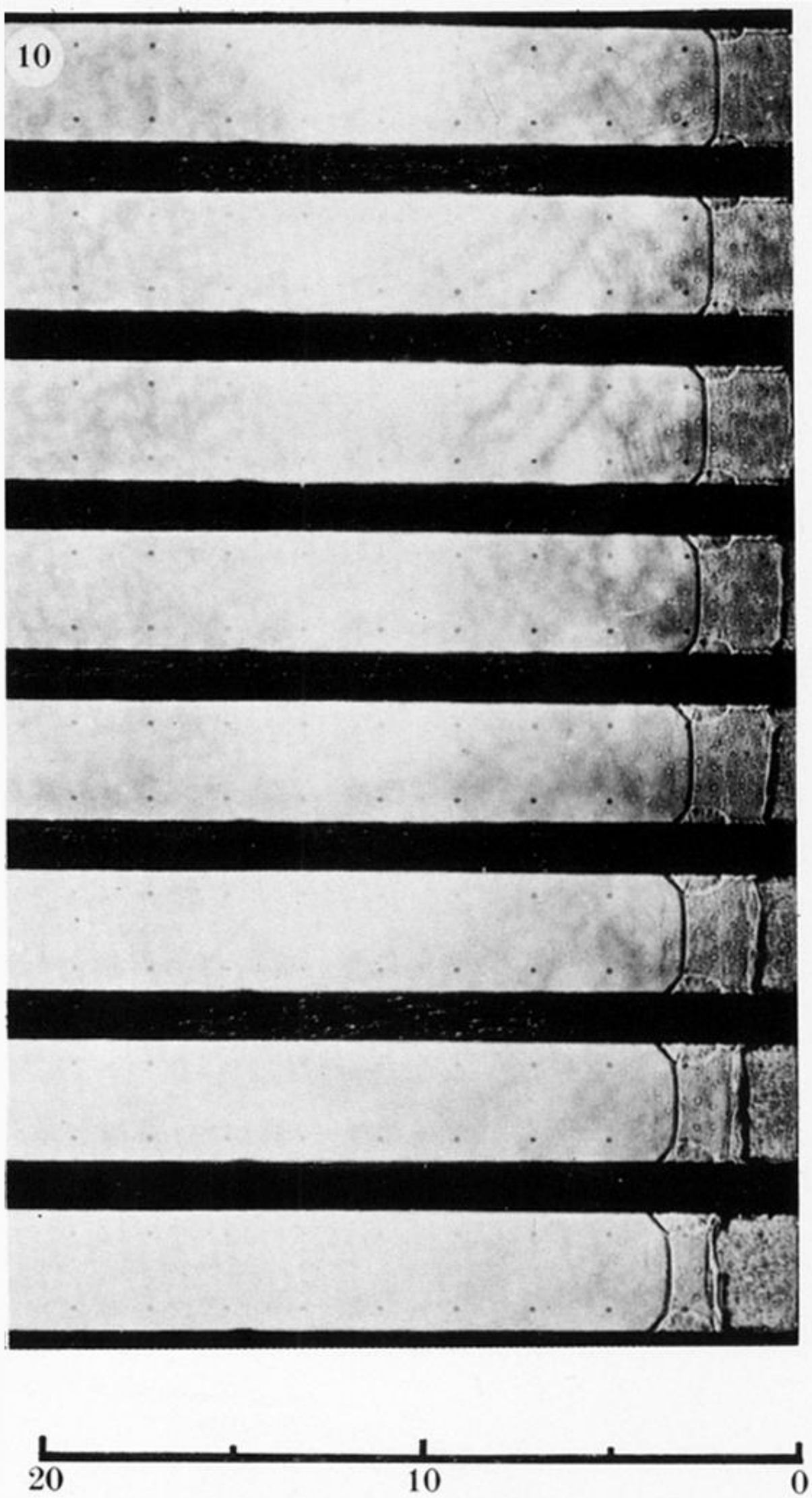

FIGURE 10. Cinematographic schlieren record of strong ignition obtained under the same conditions as figure 9 but with temperature of 1400 K (Vermeer *et al.* 1972). The photographic conditions are as in figure 9.

PHILOSOPHICAL TRANSACTIONS OF THE ROYAL SOCIETY A MATHEMATICAL, PHYSICAL & ENGINEERING SCIENCES

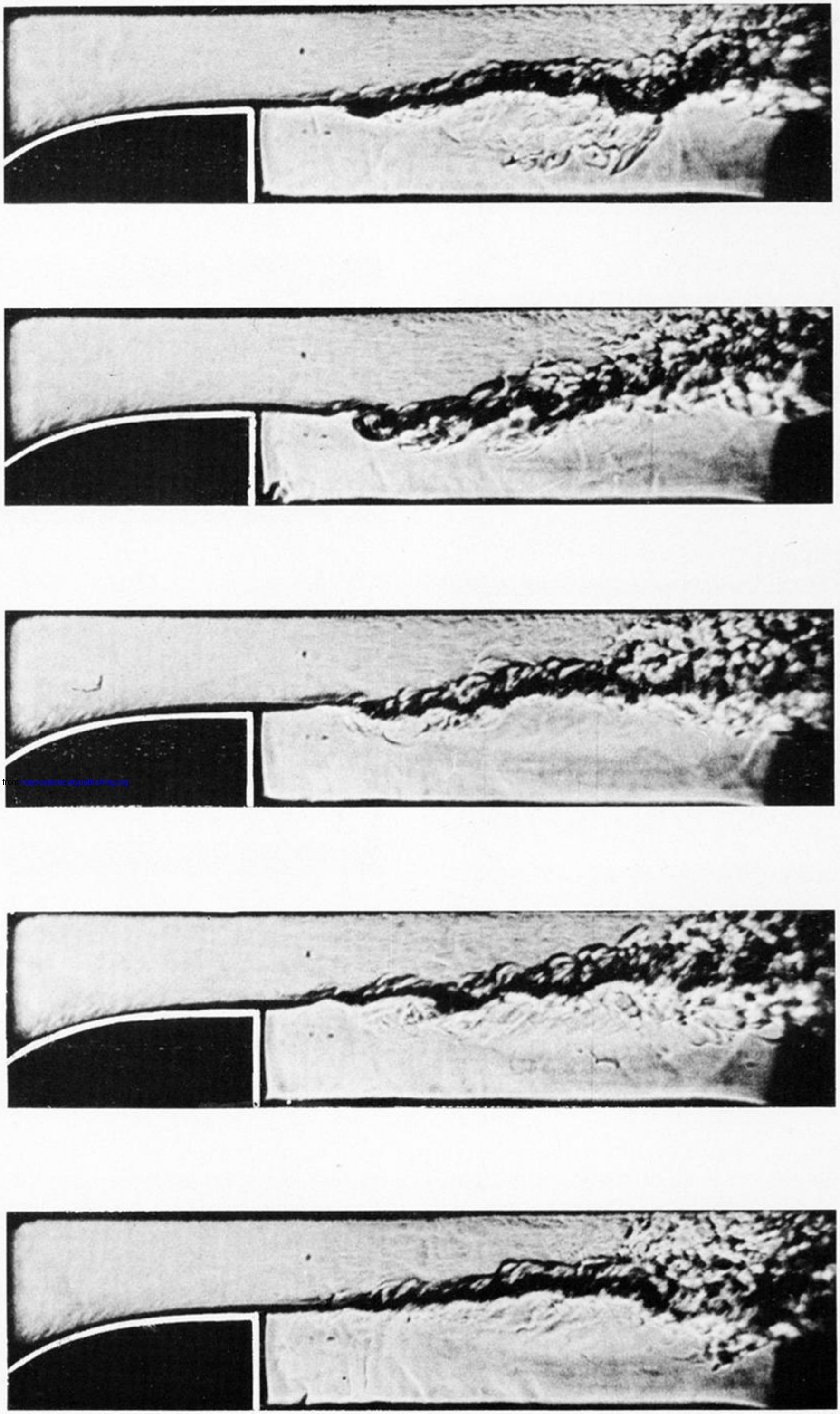

FIGURE 14. Cinematographic schlieren records of turbulent flame in a combustion tunnel. Height of channel is 5 cm. Reynolds number of flow at inlet of 5 cm is around 10^4. Sequence is from the top at intervals of around 19 ms between frames.

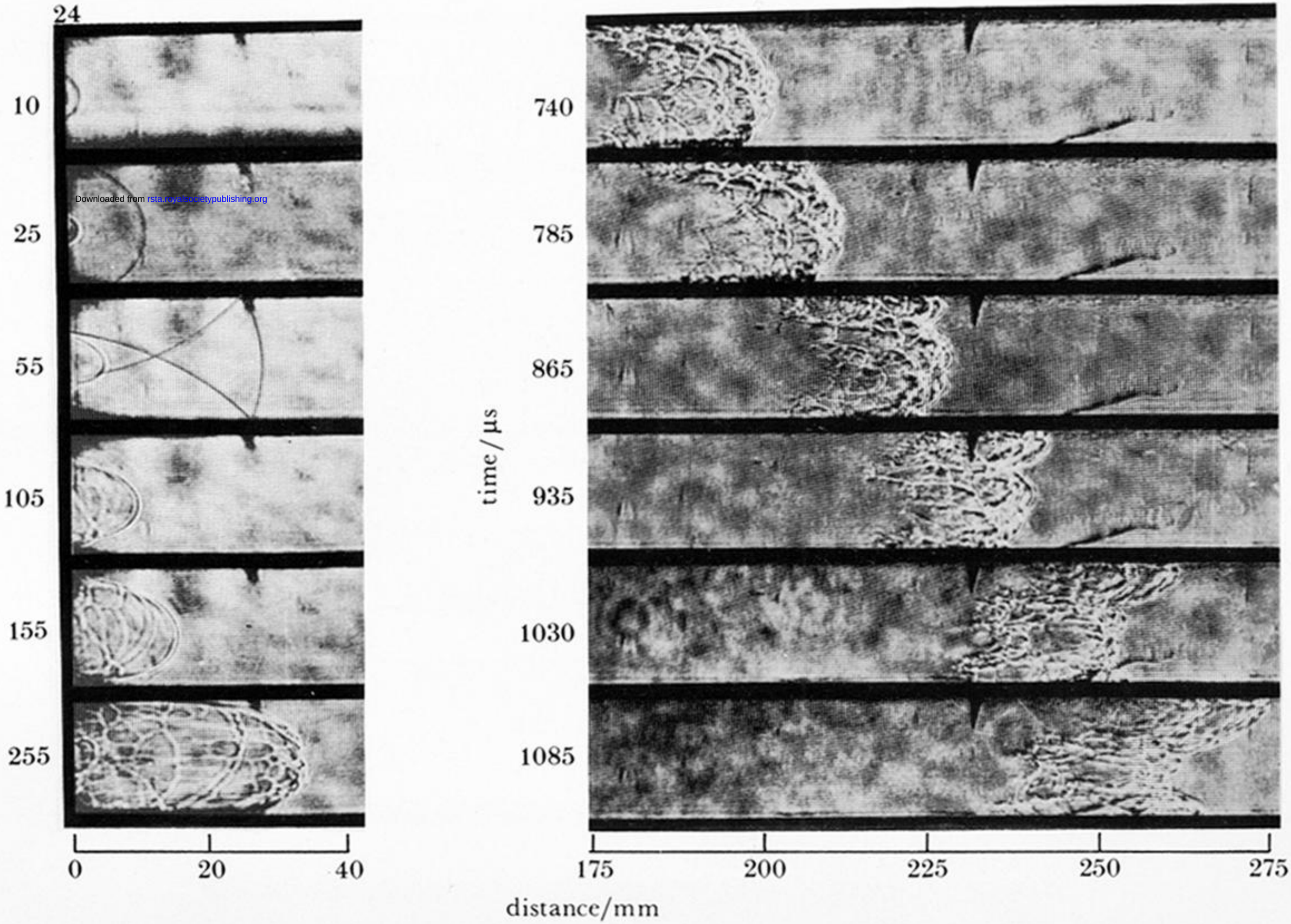

FIGURE 24. Cinematographic schlieren records of ignition, and initial stages of inflammation in a stoichiometric hydrogen–oxygen mixture.

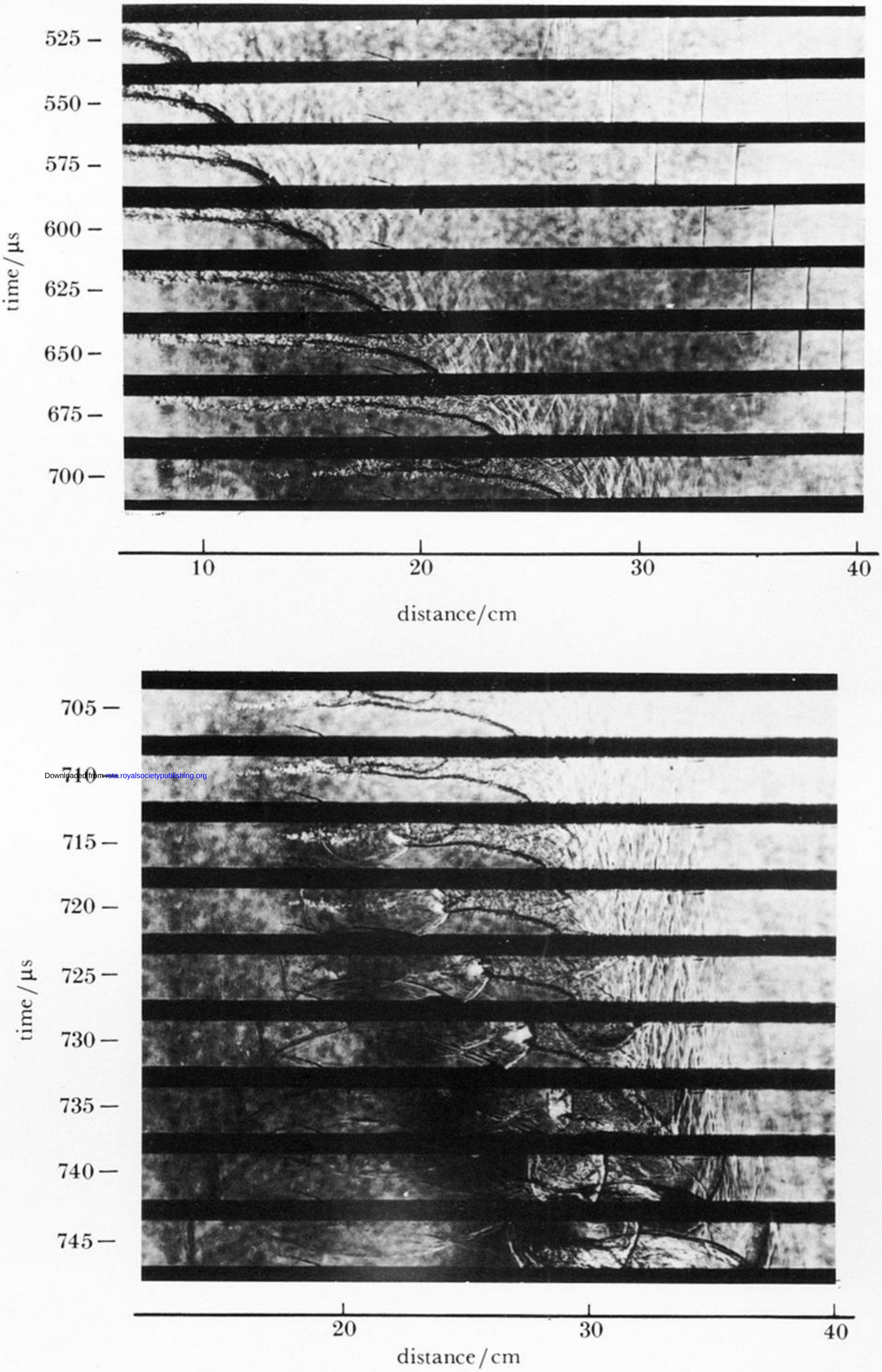

FIGURE 25. Cinematographic schlieren records of intense generation of compression waves by turbulent flame leading to the 'explosion in the explosion' that manifests the transition to detonation (Meyer *et al.* 1970). Later stages of the process depicted in figure 2.

IGURE 27. Cinematographic schlieren records of a detonation wave in its self-sustaining mode of propagation, and its imprint on a soot covered wall of a rectangular duct, displayed at top. (Oppenheim 1972).

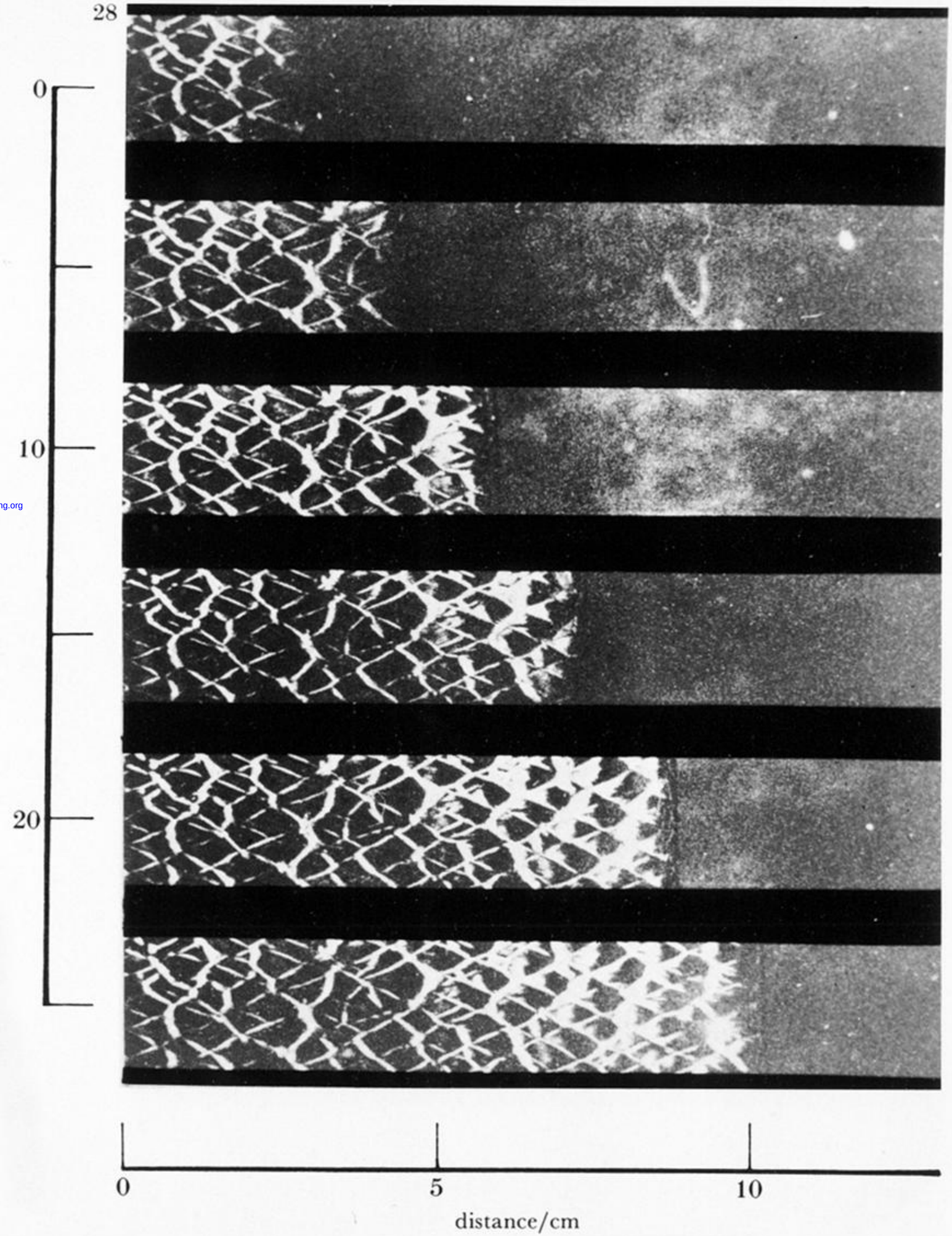

FIGURE 28. Cinematographic schlieren photographs catching the detonation wave in the act of writing on the wall (Oppenheim 1972).

PHILOSOPHICAL TRANSACTIONS OF THE ROYAL SOCIETY A MATHEMATICAL, PHYSICAL & ENGINEERING SCIENCES

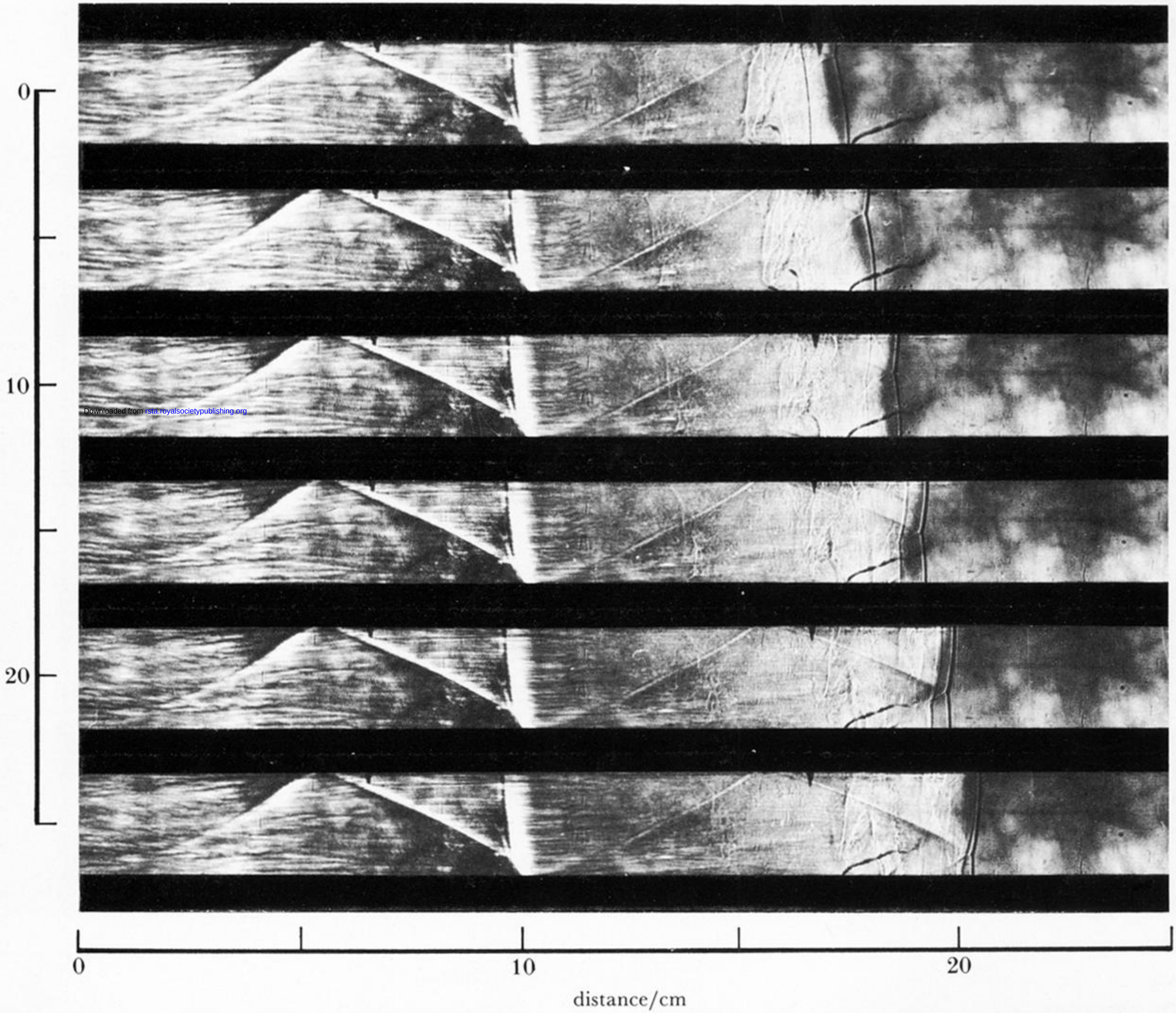

FIGURE 29. A sequence of cinematographic records that reveal the details of the detonation wave front and its action in writing the wall. Structure reduced to a single triple point intersection by proper adjustment of initial conditions (Oppenheim 1972).

PHILOSOPHICAL TRANSACTIONS OF THE ROYAL SOCIETY A MATHEMATICAL, PHYSICAL & ENGINEERING SCIENCES

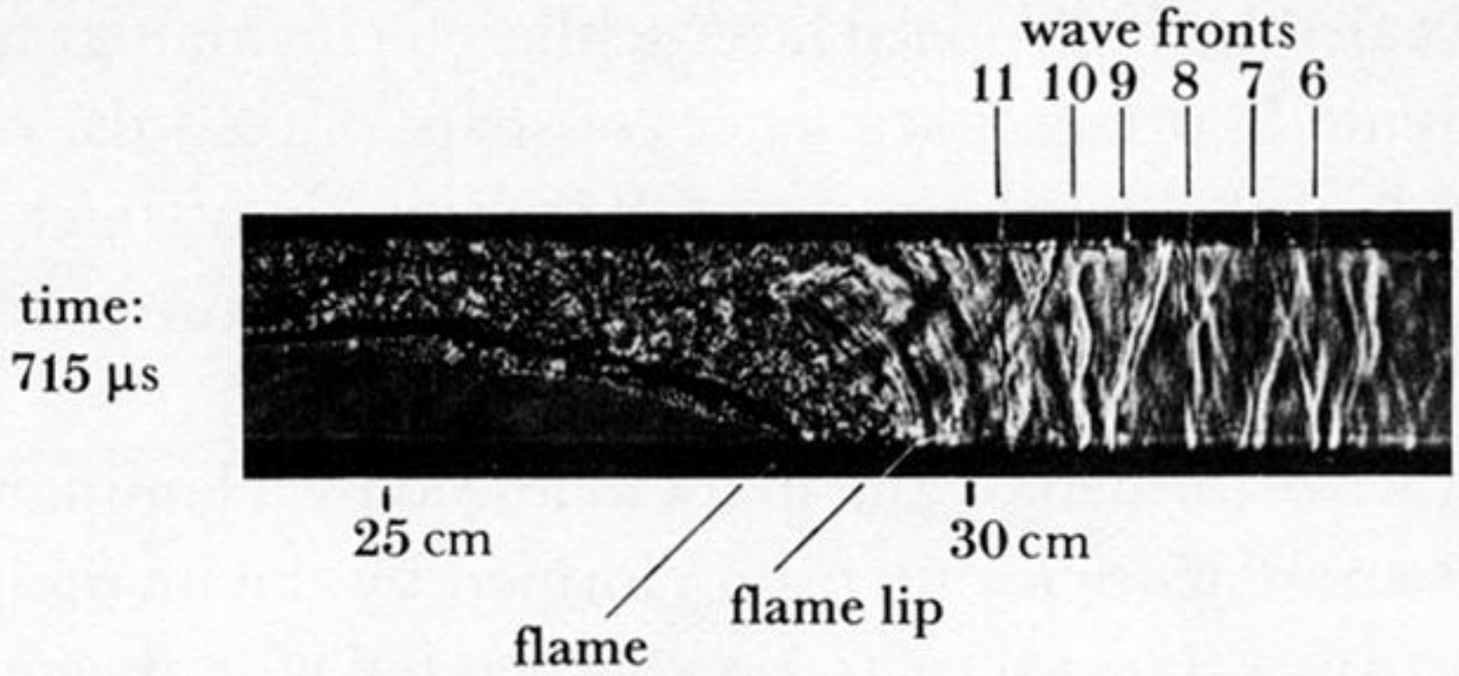

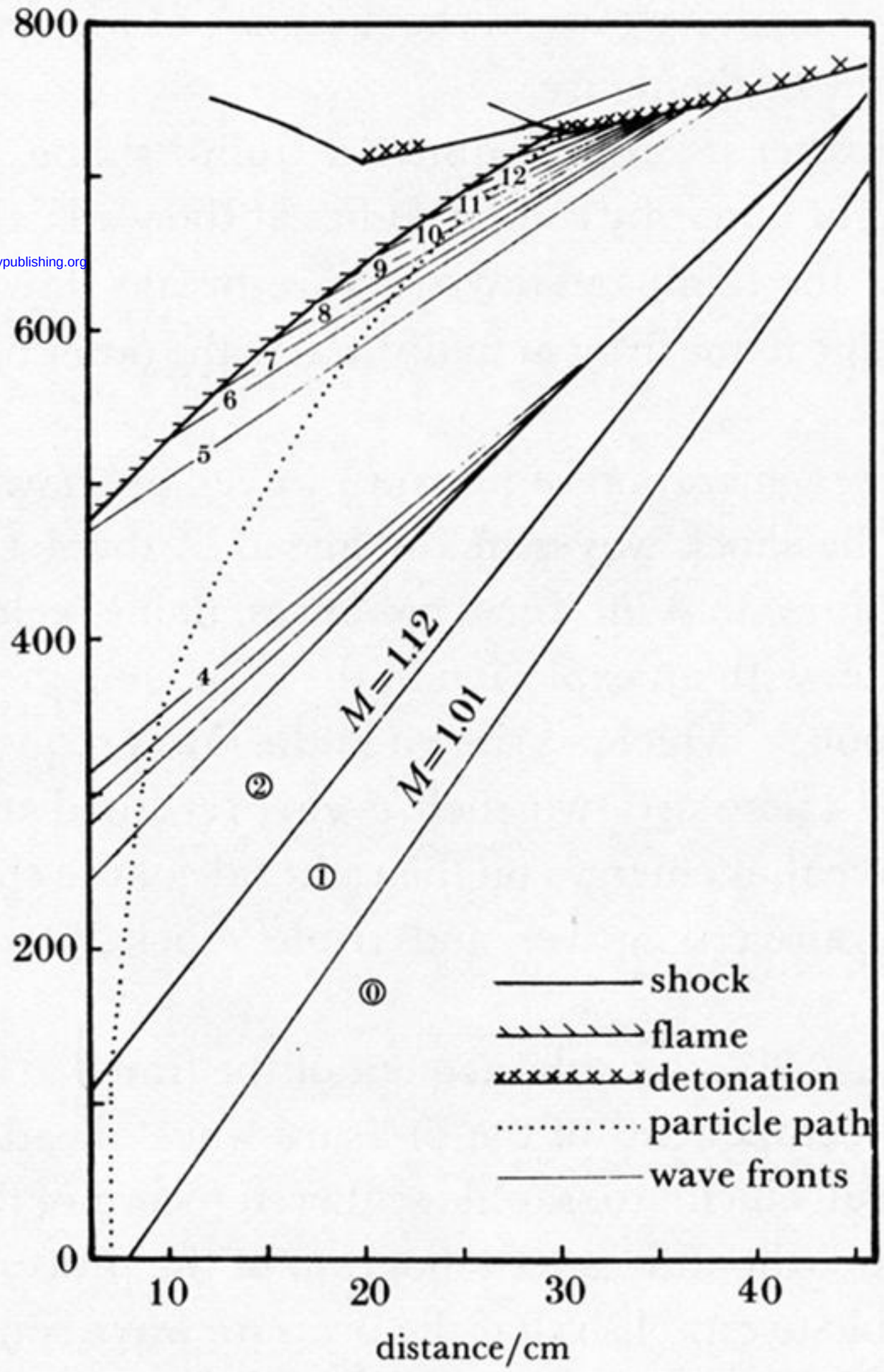

GURE 26. Time–space history of gas-dynamic processes associated with the development of detonation depicted in figure 25 (Meyer *et al.* 1970).